*Tellus (1996), 48B, 543–567*
*Printed in UK – all rights reserved*


**TELLUS**
*ISSN 0280–6509*

# Simulations of terrestrial carbon metabolism and atmospheric $CO_2$ in a general circulation model

## Part 2: Simulated $CO_2$ concentrations

By A. SCOTT DENNING[1,*], DAVID A. RANDALL[2], G. JAMES COLLATZ[3] and PIERS J. SELLERS[3], [1]*School of Environmental Science and Management, University of California, Santa Barbara, CA 93106-5131, USA;* [2]*Department of Atmospheric Science, Colorado State University, Fort Collins, CO 80521-1371, USA;* [3]*National Aeronautic and Space Administration, Goddard Space Flight Center, MS 923, Greenbelt, MD 20771, USA*

(Manuscript received 28 September 1995; in final form 15 May 1996)

ABSTRACT

The effects of terrestrial photosynthesis and respiration on the mixing ratio of atmospheric $CO_2$ have been simulated using surface fluxes calculated using a new version of the simple biosphere model (SiB2) coupled to the Colorado State University (CSU) general circulation model (GCM). The model was integrated for 5 years from an initial condition of uniform $CO_2$, with surface fluxes and atmospheric transport calculated on a 6-min time step. Subgrid-scale vertical transport includes the effects of cumulus and dry convection and boundary layer turbulence, with diurnal cycles of all processes well resolved. The amplitude and phase of the diurnal cycle of simulated $CO_2$ concentration during the growing season agreed very well with observations made in Brazil, the southeastern United States, and central Canada, and the vertical structure of the simulated diurnal variations of $CO_2$ in the lower troposphere appears to be fairly realistic. By contrast, when the model was driven with surface fluxes of $CO_2$ derived from monthly means saved from the on-line simulation, the diurnal cycle was much weaker than observed at all three locations and was nearly 180° out of phase with the observations. The amplitude and phase of the seasonal cycle of simulated concentration show good agreement with data collected in remote marine areas by the flask sampling network. Vertical attenuation of the seasonal amplitude in the model is stronger than observed, at least over the western Pacific ocean where seasonal data have been collected by aircraft. In the annual mean, correlations between the carbon fluxes and vertical atmospheric transport produce very strong concentration maxima over the tropical rain forests, but covariance of fluxes and transport on the seasonal time scale are more important in the middle latitudes. The effect of these correlations is to impose a vertical gradient of several parts per million on the zonal mean atmospheric $CO_2$ concentration over biologically active regions, with the seasonal cycle contributing about 75% of the effect and the diurnal cycle contributing about 25%. The simulated annual mean meridional gradient in concentration at the flask stations is much stronger than has been simulated with off-line tracer transport models, accounting for more than half of the observed north-south gradient.

## 1. Introduction

One of the strongest lines of evidence for a significant sink of anthropogenic $CO_2$ in the terrestrial biosphere arises from attempts to reconcile the observed distribution of global atmospheric $CO_2$ concentration with simulations using tracer transport models and various hypotheses of sources and sinks at the Earth's surface (Pearman and Hyson, 1980, 1986; Pearman et al., 1983; Tans et al., 1989, 1990; Enting and Mansbridge, 1989,

* Corresponding author.

1991; Keeling et al., 1989; Denning, 1994; Enting et al., 1995). Most studies of this kind have found a weak annual mean meridional gradient in surface concentration arising from correlations between seasonal biotic fluxes and atmospheric transport. Denning et al. (1995) have shown that when the simulated transport includes variable-depth turbulent mixing near the ground, nonlinear interactions between purely seasonal fluxes and transport impose an annual mean gradient in concentration roughly half as strong as that created by fossil fuel combustion. This effect leads to a calculated net sink in the terrestrial biosphere that is stronger than would be inferred otherwise, but depends sensitively on the seasonal timing of photosynthesis and respiration fluxes relative to vertical transport by atmospheric turbulence and moist convection (Denning, 1994; Denning et al., 1995). Because of the impact of such correlations between fluxes and transport, calculation of the global carbon budget by comparing simulated and observed $CO_2$ concentrations requires accurate simulation of the purely seasonal components of terrestrial ecosystem metabolism.

Because the diurnal variations of surface carbon exchange and atmospheric circulation are each driven by solar radiation, diurnal as well as seasonal correlations are likely to influence the spatial distribution of $CO_2$. Yet in all previous studies of the global carbon cycle using atmospheric tracer transport models, the diurnal cycle of the surface fluxes has been "averaged out," and prescribed in terms of monthly mean values. Even the diurnal cycle of atmospheric turbulence is very poorly resolved with a time step of four hours (as used by Heimann and Keeling, (1989) and Tans et al. (1990)). Previous studies have represented cumulus convection in terms of a monthly mean mixing frequency, so that vertical tracer transport has no diurnal component either. These idealizations have simplified the tracer transport problem so that the calculations are computationally efficient, but are justified only to the extent that diurnal correlations between the biological exchange of $CO_2$ and atmospheric circulation do not significantly affect the simulated tracer distribution.

In a companion paper, Denning et al. (1996) (referred to hereafter as Part 1) report on the results of simulations of land-atmosphere carbon exchange in a coupled climate-land biosphere model. They show that the coupled model captures important aspects of the terrestrial carbon cycle at the annual mean, seasonal, and diurnal time scales. In the present paper, we extend the analysis into the atmosphere itself by using the simulated carbon fluxes and the simulated circulation field of the Colorado State University (CSU) general circulation model (GCM) to drive prognostic calculation of the atmospheric mixing ratio of $CO_2$. Comparison of the simulated $CO_2$ concentrations to observations allows us to simultaneously validate both the simulated carbon fluxes presented in Part 1 and the simulated atmospheric transport in the GCM. In addition, we perform a sensitivity experiment in which the fluxes derived by SiB2 are prescribed without a diurnal cycle to investigate the impact of the diurnal coupling of subgrid-scale vertical transport in the GCM with the carbon fluxes simulated by SiB2. Only the effects of carbon exchange between the atmosphere and the land surface are simulated here; no attempt is made to represent the fluxes due to anthropogenic emissions, air-sea exchange, or chemical transformations within the atmosphere.

In Section 2, we describe the tracer transport calculation and the coupling between the ecosystem metabolism and simulated concentration field. Simulated transport and concentration fields are analyzed and compared to observational data in Section 3 for the diurnal cycle, in Section 4 for the seasonal cycle, and in Section 5 for the annual mean. Calculation of the annual carbon budget of the atmosphere using these results is beyond the scope of the present paper, but is an objective of the research program described here (Denning, 1994).

## 2. Methods

The climate simulation in the CSU GCM is described briefly in Part 1, and will not be discussed further here. Recent model results are presented by Randall et al. (1989, 1991, 1996), Stephens et al. (1993), and Fowler and Randall (1996). In this section we describe the tracer transport calculation used to determine the three-dimensional concentration field of atmospheric $CO_2$ at each model time step and the experiments we performed.

*2.1. Tracer transport calculation*

The time rate of change of the mixing ratio $C$ of $CO_2$ in the atmosphere can be written as

$$\frac{\partial}{\partial t}(\bar{\rho}\bar{C}) = -\nabla\cdot(\bar{\rho}\bar{C}\bar{V}) - \nabla\cdot(\rho'\overline{C'V'}) + F_C, \qquad (1)$$

where $C$ is the $CO_2$ mixing ratio, $\rho$ is the density of the air, $V$ is the three-dimensional wind vector, and $F_C$ is a boundary flux at the Earth's surface. The overbars indicate grid cell mean quantities and the primes indicate subgrid-scale deviations from these means. The first term on the right-hand side of (1) refers to explicitly resolved tracer transport (advection) by the mean flow, and the second term to parameterized processes affecting the concentration that occur at spatial scales too small to be explicitly resolved by the model. Subgrid-scale fluxes represented in the model include turbulent diffusion in a well mixed planetary boundary layer, vertical mixing due to dry convection, and vertical transport by penetrative cumulus convection. Convection resulting from instability in higher layers is parameterized by a moist adjustment process (Manabe et al., 1965), but we have not attempted to represent vertical transport of $CO_2$ by this process. Exchanges of mass between the PBL and the free troposphere also occur in the model in the presence of boundary layer clouds. This process is referred to as "layer cloud instability" (Suarez et al., 1983). For simplicity, we have neglected its effect on the simulated tracer concentrations.

The concentration $C$ in (1) is not allowed to affect the simulated transport in any way, and nonlinear products of $C$ do not appear, so (1) is linear in $C$. This means that the total concentration of $CO_2$ in the model can be separated into arbitrary components which are treated separately in terms of their surface fluxes and transport, allowing separate analysis of the effects of fossil fuel emissions, exchange with certain regions of the oceans, or $CO_2$ fertilization, for example. This separability is the basis for "synthesis inversion" studies (Tans et al., 1989, 1990; Enting and Mansbridge, 1989, 1991; Keeling et al., 1989; Denning, 1994; Enting et al., 1995), in which linear combinations of the various components are constructed to match the observed spatial and temporal variations of $CO_2$. In the present study, we represent $F_C$ only in terms of seasonal photosynthesis and respiration at the land surface (see Part 1), neglecting all other sources and sinks (such as fossil fuel emissions, air-sea exchange, and land use change). Volumetric sources and sinks due to chemical reactions (such as oxidation of methane and other organic compounds) are also neglected.

*2.1.1. Advection by the mean flow.* Horizontal advection of $CO_2$ is calculated by a second-order, centered-in-space, leapfrog-in-time scheme. We recognize that this scheme is prone to dispersion errors in the presence of strong gradients (Rood, 1987), but since the $CO_2$ tracers were integraed from a globally uniform initial condition and the surface flux of $CO_2$ produces fluctuations that are more than an order of magnitude smaller than the "background" concentrations, this was generally not a problem. Above the top of the PBL, vertical advection of $CO_2$ is represented by a centered-in-space, leapfrog-in-time scheme. At the PBL top, a 1st-order upstream scheme is applied separately for turbulent entrainment and loss of tracer mass from the PBL due to cumulus mass flux. After each 10 leapfrog timesteps, we perform a Matsuno step to suppress the computational mode (Arakawa and Lamb, 1977).

*2.1.2. Planetary boundary layer.* A key feature of the CSU GCM is its formulation in terms of a modified sigma coordinate, in which the PBL top is a coordinate surface, and the PBL itself is the lowest model layer (Suarez et al., 1983; see Fig. 1). The PBL depth is calculated prognostically from

$$\frac{\partial}{\partial t}(\pi_M) + \nabla\cdot\left(\int_1^2 \pi_M V\, d\sigma\right) = g(E - M_B), \qquad (2)$$

where $\pi_M \equiv \rho_S - \rho_B$ is the pressure thickness of the PBL, $E$ is the rate of turbulent entrainment at the PBL top, and $M_B$ is the mass flux into the base of cumulus clouds, which is calculated by the cumulus parameterization. Mass sources and sinks for the PBL consist of large-scale convergence or divergence, turbulent entrainment, and the cumulus mass flux. The turbulence kinetic energy (TKE, denoted by $e_M$) of the PBL has recently been introduced as a new prognostic variable, simplifying the entrainment calculation (Randall et al., 1992). Turbulent entrainment can be driven by positive buoyancy fluxes, or by shear of the mean wind in the surface layer or at the PBL top,

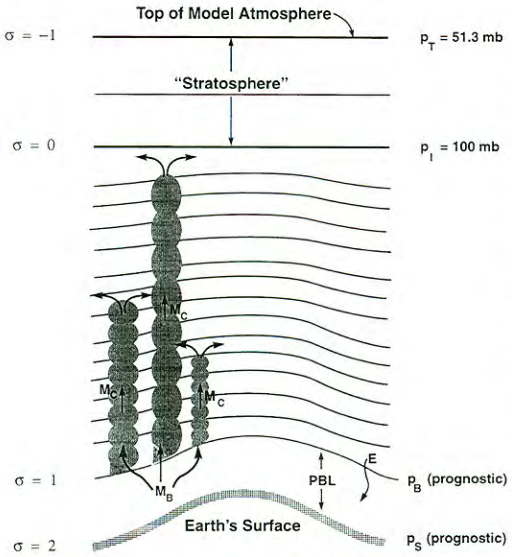


*Fig. 1.* Vertical structure of the CSU GCM. Symbols are defined in the text.

and is derived from the prognostic equation for the TKE, which is

$$g^{-1}\pi_M \frac{\partial e_M}{\partial t} + Ee_M = B + S - D, \tag{3}$$

where $B$ and $S$ represent TKE production by buoyancy fluxes and shear, respectively, and $D$ represents dissipation.

The time rate of change of the mean mass mixing ratio of $CO_2$, $C_M$ in the PBL is given by

$$\frac{\partial}{\partial t}(\pi_M C_M) + \nabla\cdot(\pi_M \mathbf{V} C_M) = (\pi_M \dot{\sigma})_{B+} C_{B+} - gM_B(C_{Cu} - C_{B+}), \tag{4}$$

where $C_{B+}$ is the grid cell mean mixing ratio just above the PBL top, $C_{Cu}$ is the mixing ratio in cumulus cloud, **V** is the horizontal (vector) wind, and

$$\frac{1}{g}\pi_M \dot{\sigma} = E - M_B \tag{5}$$

is the downward mass flux across the PBL top. Recall that the PBL top is a coordinate surface (Fig. 1), but that the physical depth of the turbulent PBL changes due to turbulent entrainment ($E$), which can be negative, loss of mass into cumulus clouds ($M_B$), and horizontal divergence or convergence of mass.

*2.1.3. Vertical transport by cumulus convection.* In the cumulus parameterization of the CSU GCM, an ensemble of clouds of multiple depths is considered to exist in those model columns in which cumulus convection occurs (Arakawa and Schubert, 1974; Lord et al., 1982; Randall and Pan, 1993). The clouds all originate at the top of the PBL and extend to some (or even all) of the other layer-tops in the model atmosphere. The model calculates the amount of cumulus available potential energy in a grid column, and then apportions the release of this energy into one or more "types" of clouds defined by the fractional amount of entrainment of environmental air into the cloud as it passes through each layer. The fractional entrainment rate is assumed to be independent of height. In-cloud air in each type of cloud has the properties of the PBL at cloud base, but is altered by entrainment in each layer through which it passes. The top of each cloud type is determiend by the level at which the in-cloud air (now diluted by entrainment) becomes neutrally buoyant with respect to the environment. The mass flux, $M_C$, due to each cloud type at the base of each layer in each grid column (Fig. 2) is calculated by the Arakawa-Schubert parameterization. The availability of this mass flux makes calculation of the vertical transport of atmospheric tracers quite straightforward, and is one of the strengths of this cumulus parameterization.

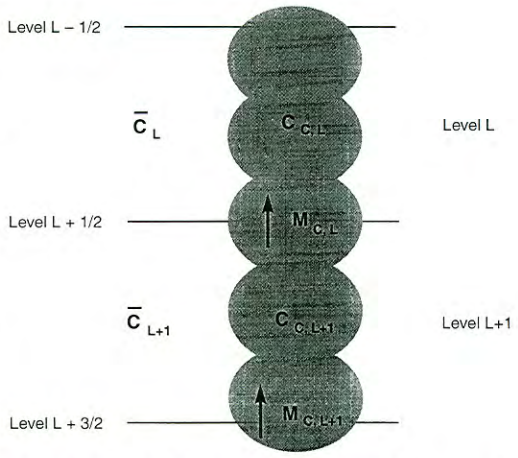


*Fig. 2.* Schematic diagram of relationships between variables used to simulate vertical tracer transport by cumulus convection in the CSU GCM. Symbols are defined in the text.

The in-cloud air at the top of the PBL is assumed to have the tracer concentration of the PBL, since all the cloud air is drawn from the PBL. At each successive layer base above the PBL top, the in-cloud tracer concentration is calculated for each cloud type as

$$C_{C,L} = \frac{C_{C,L+1} + \bar{C}_{L+1}\lambda\delta z}{1+\lambda\delta z}, \tag{6}$$

where $C_{C,L}$ is the in-cloud concentration at level $L$, $\bar{C}_L$ is the environmental concentration of the tracer (outside the cloud) at level L, and

$$\lambda\delta z \equiv \frac{M_{C,L} - M_{C,L+1}}{M_{C,L+1}} \tag{7}$$

is the fractional entrainment rate of the cloud. The flux of each tracer into each model layer due to cumulus convection is simply $M_C(C_C - \bar{C})$, the product of the cumulus mass flux into the layer and the difference in tracer concentration between the in-cloud air and the environmental air at that level. This calculation is performed for each level up to the top of each cloud, and the fluxes were summed over all types (top-heights) of cloud present in the given grid column. The change in tracer concentration due to cumulus convection is then calculated as the divergence of the total tracer flux due to all cloud types. This calculation is performed only once per simulated hour, and one tenth of the change in concentration is applied incrementally in "eyedropper" fashion every six minutes.

*2.1.4. Vertical transport by dry convection.* Vertical transport of $CO_2$ due to mixing by dry convection is calculated as follows. After horizontal and vertical advection is performed in the dynamics routine (every 6 min), each column of air in the model is checked for unstable pairs of layers. If at least one pair of unstable layers ($\theta_L < \theta_{L+1}$) is found in a column, the column is examined in detail to find the upper and lower bounds of the unstable layer(s). In each unstable region, the total mass of the region and of each tracer is determined. The concentration of each tracer at each model level in the unstable region is then set to the mass of the tracer in the unstable region divided by the mass of the region. This process is repeated until the entire column is statically stable. This process is important over arid land areas (such as the Sahara) where surface heating is strong but there is little water vapor in the PBL to allow cumulus convection. This situation is essentially an extension of the PBL, which is needed because the lowest model layer is not allowed to occupy more than 20% of the depth of the troposphere to prevent excessive loss of vertical resolution.

### 2.2. *Surface carbon fluxes*

Unlike previous studies of tracer transport (including Denning et al., 1995), we do not prescribe surface exchanges of $CO_2$ from boundary conditions given a priori, but rather determine them on-line in the GCM (see Part 1). An important consideration is that gross photosynthesis and ecosystem respiration be balanced (or nearly so) over the annual cycle to avoid large regional sources or sinks of $CO_2$ to the atmosphere which might impose unrealistic spatial structures on the concentration field. This is accomplished by calculating $CO_2$ efflux due to soil respiration using a nondimensional rate (at each model grid cell and time step), defined as

$$r(x, t) = \frac{R^*(x, t)}{\sum_{1\ \text{year}} R^*(x, t)\Delta t}, \tag{8}$$

where $R^*$ is a diagnostic function of soil moisture and soil temperature (Part 1). The dimensional carbon flux due to respiration is then determined by multiplying this rate by the annual integral of canopy net assimilation at each grid cell,

$$R(x, t) = r(x, t) \int_{1\ \text{year}} A_c(x, t)\, \mathrm{d}t. \tag{9}$$

The approach outlined above produces exact annual carbon balance at every model grid point when used as a diagnostic tool to process model output, as we have done in Part 1. Some modification is required to use this method to calculate $CO_2$ concentraions on-line, because the annual sums of $A_C$ and $R^*$ cannot be calculated a priori. Instead, they are computed at each grid cell at the end of each year of the integration and then used during the following year. Conceptually, this means that all carbon sequestered by photosynthesis in a given year is released back to the atmosphere in the following year. A small net source or sink for atmospheric $CO_2$ occurs wherever there is significant interannual variability in

annual net assimilation or $R^*$, but as long as there is no secular trend, the overall effect of the simulated fluxes is very close to neutral with respect to atmospheric $CO_2$ over a period of several years.

The calculation of the stomatal conductance and assimilation rate in SiB2 involves the partial pressure of $CO_2$ in the intercellular spaces of the plant canopy (Sellers et al., 1996). This value is diagnosed from a number of other quantities, including the concentration of $CO_2$ in the atmospheric mixed layer, which is treated as a prognostic variable in the present study. It is likely that significant feedback occurs between the rate of carbon assimilation by photosynthesis and atmospheric $CO_2$ concentrations near the surface, both in the real world and potentially in SiB2. For simplicity, we have chosen not to represent this feedback in the calculations presented here, but rather have allowed the interaction between ecosystem processes and atmospheric $CO_2$ to operate in only one direction. Changes in photosynthetic assimilation will therefore affect atmospheric $CO_2$, but a constant mixed layer concentration of 350 parts per million by volume (ppm) is specified in SiB2. Inclusion of the effects of atmospheric $CO_2$ on the simulated biochemistry and physiology would be straightforward to implement in SiB2, but would have complicated the interpretation of the results of this initial set of experiments.

At ocean grid cells, the surface carbon flux is assumed to be zero in the experiments presented here. We also do not consider the effects of fossil fuel combustion, tropical deforestation, $CO_2$ fertilization, or any other process than annually balanced terrestrial ecosystem exchange.

### *2.3. Experimental integration*

Because of the 1-year lag between the simulated fluxes due to assimilation and respiration, the model was "spun up" for one annual cycle to provide the necessary antecedent conditions for the respiration calculation in (9). At that point, the tracer calculation was begun with an initial condition of globally uniform $CO_2$ concentration of 350 ppm, and the model integrated for four more years on the standard CSU GCM grid of $4° \times 5°$ with 17 levels, using a time step of 6 min. The first 3 years of the tracer simulation are regarded as an initialization period in which the simulated concentration field adjusted to the surface fluxes provided by SiB2. Except as noted otherwise, results presented here are monthly means for the final year of the simulation.

To investigate the effect of the resolved diurnal variations of the carbon fluxes on the simulated concentration field, we performed a second experiment in parallel with the integration described above (referred to as the "SiB2" experiment). In this sensitivity run (which we refer to as the "meanSiB" experiment), we saved the monthly mean fluxes of $CO_2$ to the atmosphere generated by SiB2 and prescribed them as a boundary condition to the atmospheric tracer calculation, as has been done for other seasonal carbon flux maps in previous studies (Fung et al., 1983, 1987; Heimann and Keeling, 1989; Tans et al., 1990; Denning 1994; Denning et al., 1995). Constant fluxes were assigned for each grid point at day boundaries by linear interpolation between monthly mean values, which were assigned to the 15th of each calendar month.

For computational efficiency, the mean fluxes for a given year were run in the GCM during the following year of integration, concurrent with the calculation of a new set of flux data. At the end of the fourth year of the SiB2 integration, only 3 years of meanSiB had been run, so the final year was repeated using the monthly mean fluxes to drive the meanSiB calculation. Results from this final year are used to compare diurnal cycles at specific grid points; in this way, both the circulation and surface carbon fluxes are identical, allowing a meaningful comparison of the simulated concentrations between the two experiments.

## 3. Diurnal cycle

The use of diurnally varying carbon fluxes at the land surface and a time step which resolves the diurnal cycles of atmospheric circulation are the most significant new features of the present study relative to previous simulations of global $CO_2$ concentration and transport. The implications of these coupled diurnal cycles on the global scale remains to be seen, but the realism of any global effects hinges on the ability of the model to reasonably reproduce the behavior of the surface fluxes, atmospheric properties, and $CO_2$ concentrations on the local scale. In Part 1, we showed

that the diurnal cycle of terrestrial carbon metabolism is reasonably well simulated by SiB2 at several locations where field data are available, although we noted a tendency of the model to underestimate the midday uptake of $CO_2$ due to excessive moisture stress. In this section we examine the simulated diurnal cycle of the $CO_2$ concentration at a number of locations, paying particular attention to coupling between subgrid-scale vertical transport and $CO_2$ concentration.

Near Manaus, Brazil, the diurnal cycles of $CO_2$ flux and concentration were documented for July of 1985 and May of 1987 during the Amazon Boundary Layer Experiment (ABLE) (Wofsy et al., 1988; Fan et al., 1990). In Part 1, we showed that simulations of $CO_2$ fluxes by SiB2 reproduced the phase of the diurnal cycle at this location quite well, but underestimated its amplitude by nearly 50% in May. In Fig. 3, we present composite diurnal cycles of a number of near-surface variables for July of the final year of the simulation, derived by averaging the values of each variable for each hour of the day across the month.

The $CO_2$ flux to the atmosphere simulated by SiB2 (Fig. 3a) is nearly constant at night (about 3 $\mu$Mol m$^{-2}$ s$^{-1}$), then becomes negative around sunrise and reaches a relatively steady value of about $-10$ $\mu$Mol m$^{-2}$ s$^{-1}$ by late morning. In late afternoon, photosynthetic uptake ceases and the flux becomes positive again about sunset. The depth of the turbulent PBL (into which the simulated fluxes are "mixed") follows a similar cycle (Fig. 3b) with stable nocturnal conditions restricting mixing to about 100 m, followed by rapid growth by turbulent entrainment in mid to late morning, reaching a maximum of about 900 m in mid afternoon. Surface cooling in the evening causes the turbulence to collapse (due to "negative entrainment" in the terminology of Suarez et al. (1983)), with the PBL depth decreasing to about 100 m by 20:00 local time. There is a lag of about three hours betwee the start of simulated photosynthesis at sunrise and the period of rapid turbulent entrainment before surface heating is sufficient to break the nocturnal temperature inversion. For this particular grid point and month, cumulus convection shows a very strong maximum at 11:00 (Fig. 3c), with weaker activity through the afternoon hours and practically no convection at night.

The $CO_2$ concentration simulated by SiB2 shows a diurnal oscillation with amplitude of 32 ppm, with the maximum occurring at sunrise and the minimum occurring in late afternoon (Fig. 3d). By contrast, for the meanSiB experiment in which the fluxes were prescribed as monthly means, the simulated $CO_2$ (Fig. 3d) had a minimum around 19:00 and a maximum about 15:00 local time. The amplitude of the diurnal cycle was much less (5 ppm) in the meanSiB experiment than as simulated by SiB2. Aircraft data intended to represent the vertically integrated PBL concentration (Wofsy et al., 1988) show rapidly declining concentrations through the morning hours (Fig. 3f) and steady concentrations during the afternoon. Like the SiB2 simulation, observed afternoon concentrations in the PBL were about 30 ppm lower than early morning values.

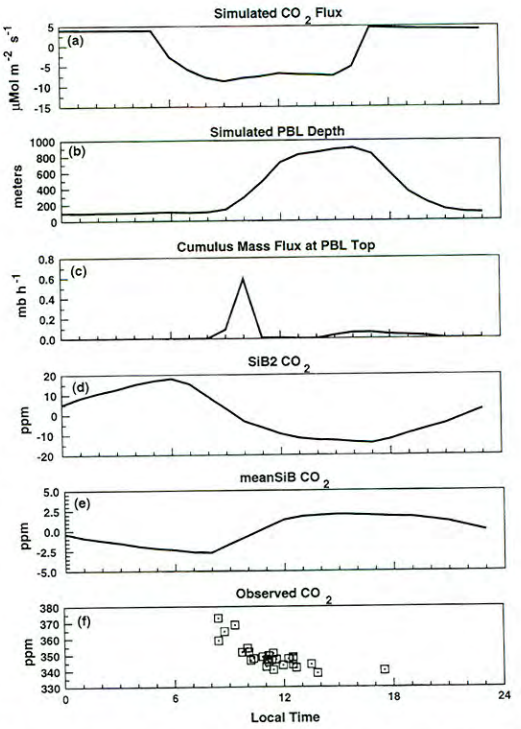


*Fig. 3.* Diurnal time series of PBL quantities over Manaus Brazil (monthly composite for July). (a) Simulated $CO_2$ flux to atmosphere ($\mu$Mol m$^{-2}$ s$^{-1}$). (b) PBL depth (m). (c) Cumulus mass flux at the PBL top (mb h$^{-1}$). (d) $CO_2$ concentration (ppm minus daily mean) simulated using SiB2. (e) $CO_2$ concentration (ppm minus daily mean) simulated in the meanSiB experiment. (f) Observed $CO_2$ concentration (ppm, PBL integral) from aircraft data (Wofsy et al., 1988).

The peculiar behavior of the simulated $CO_2$ in the meanSiB experiment is due to the lack of diurnal variations in the prescribed surface flux, coupled with diurnal variations in mixing depth in the GCM. During the growing season, net uptake continues day and night in this scenario, and since the flux acts on a shallow stable layer, concentrations are strongly depleted at night. In the morning, entrainment of nondilute air from aloft causes concentrations to rise. The phase of the diurnal $CO_2$ concentration as simulated in the meanSiB run follows that of the PBL depth, whereas the phase in the SiB2 run is dominated by the timing of the carbon flux. The diurnal concentration cycle is clearly more realistic in the SiB2 scenario.

In Fig. 4, we present the $CO_2$ concentration simulated for the ABLE grid point as a function of both local time and height above the surface. Here the means for each hour are computed for each model level and then linearly interpolated in height, but the "well-mixed" value of the PBL is substituted when a given height was less than the PBL depth. As seen above, surface concentrations are elevated (to about 380 ppm) in early morning, then decrease rapidly during the morning hours as photosynthesis consumes $CO_2$ and turbulent entrainment introduces lower concentration air from aloft. By midafternoon, the mixed layer grows to about 900 m depth, and the concentration has fallen to 348 ppm. After sundown, the buoyancy flux at the surface becomes negative and the PBL collapses, and soil respiration once again begins enriching the $CO_2$ concentration at the surface. A residual layer of air above the PBL top is "left over," with low $CO_2$ concentrations still reflecting daytime conditions in the PBL. This leads to a very strong nocturnal "$CO_2$ inversion," characterized by a gradient in $CO_2$ concentration of nearly 30 ppm across the PBL top by morning. No such "inversion" occurs in the meanSiB simulation, because there is no diurnal variation in the surface fluxes.

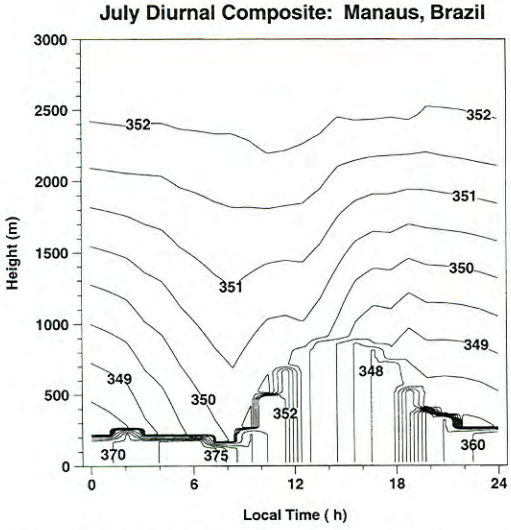


*Fig. 4.* Time-height cross section of simulated $CO_2$ concentration in the lower troposphere over Manaus, Brazil (monthly composite for July).

The vertical structure during July over the Brazilian rainforest as documented by Wofsy et al. (1988) underwent a diurnal evolution very similar to that simulated using SiB2. The aircraft data also show a "$CO_2$ inversion" of about 30 ppm in the early morning, and the "relic" depression in concentration above the nocturnal boundary layer. The mixing of the $CO_2$-depleted relic boundary layer air into the free troposphere during the night is likely to be important in controlling the long-range transport and vertical propagation of the signal from daytime photosynthesis throughout the troposphere. Furthermore, because cumulus convection is also strongly diurnal, it is likely to systematically transport low concentration air to the upper troposphere. In the mean SiB experiment, by contrast, PBL air carried aloft by cumulus convection during the growing season is systematically higher in concentration than the daily mean.

Since 1992, $CO_2$ concentration has been measured continuously at 51 m, 123 m, and 496 m above the ground on a television transmitter tower in eastern North Carolina (35° N, 77° W) in a mixed temperate forest/agricultural region (Bakwin et al., 1995). Because these data include diurnal cycles of $CO_2$ concentrations at several heights, they are a good test of the model's simulation of both the fluxes and vertical transport. In Fig. 5, we present diurnal composites of several variables for June of the final year of the simulation. As in the tropics, the simulated $CO_2$ flux (Fig. 5a), PBL depth (Fig. 5b) and cumulus mass flux (Fig. 5c) are correlated at this location. In order to compare the simulated concentratoins to the tower observations, we have not substituted

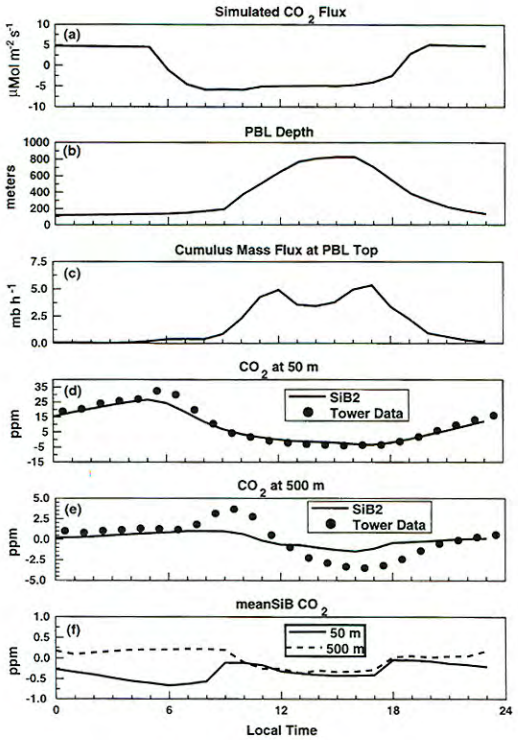


*Fig. 5.* Diurnal time series of PBL quantities over North Carolina (monthly composite for June). (a) Simulated $CO_2$ flux to atmosphere ($\mu$Mol $m^{-2}$ $s^{-1}$). (b) PBL depth (m). (c) Cumulus mass flux at the PBL top (mb $h^{-1}$). (d) $CO_2$ concentration (ppm) at 50 m above surface (simulated and observed). (e) $CO_2$ concentration (ppm) at 500 m above surface (simulated and observed). (f) $CO_2$ concentration (ppm) as simulated by meanSiB at 50 and 500 m above surface. Tower data were provided by Peter Bakwin (personal communication), and represent deviations from each day's mean concentration at 496 m, averaged across three years' of June measurements. Simulated concentrations were linearly interpolated in height, then averaged for each hour for a single month. They are normalized by the daily mean concentration at 500 m.

PBL values for composite hourly concentrations as we did above for the ABLE data (Fig. 4). Although the model does not simulate vertical structure in the concentration field within the PBL, the depth of the PBL varies for a given time of day throughout the month, so that on some days the value at 500 m (for example) represents a mixed layer value and on other days it lies in the next model layer above the PBL. At 50 m above the ground, the values presented (Fig. 5d) are always PBL-mean values, with maximum concentrations occurring about sunrise, and minimum concentrations (about 30 ppm lower) occurring about 17:00. The agreement with the tower data is excellent.

At 496 m above the ground, the tower data show much less diurnal amplitude (about 7 ppm), and the time of maximum concentration occurs about 4 h later than it does at 51 m (Fig. 5e). The simulated concentration also shows reduced amplitude and delayed phase at 500 m relative to 50 m, but the amplitude is too small (about 3 ppm). The observed vertical gradient in midafternoon is only about 2 ppm (higher at 496 m), confirming that $CO_2$ is fairly well mixed in the PBL at this location. As at the tropical site, the simulated diurnal cycle in the meanSiB experiment is characterized by reversal of the sign of the surface variations relative to both the SiB2 run and the observations (Fig. 5f), and a drastic underestimation of the amplitude.

At the site of the BOREAS Northern Study Area (Sellers et al., 1995), the diurnal cycle of $CO_2$ concentration observed (data provided by S. C. Wofsy et al., Harvard University, pesonal communication) at 30 m height is reasonably well simulated by SiB2 (Fig. 6), but the simulated concentration maxima occur too early in June and July relative to the observations. The July amplitude is observed to be about 18 ppm, but in the SiB2 simulation is only about 12 ppm. The concentrations simulated in the meanSiB experiment once again are out of phase with the observations and the SiB2 simulation during the growing season, with generally lower amplitude as well. The depth of the early morning concentration minimum as simulated by meanSiB is indicative of the strength of the monthly mean net sink; in August, it is nearly zero and by September it has become a maximum and appears to match the observations better. This corresponds to a change in the sign of the monthly mean net flux at this grid cell, with respiration dominating over photosynthesis in early autumn.

We have shown that the diurnal cycle of $CO_2$ concentration as simulated by SiB2 is quite realistic, especially as compared to the meanSiB experiment. The fluxes calculated by SiB2 represent not only the *seasonal* oscillation between photosynthesis and respiration, but also the *diurnal* cycle in which photosynthesis is active

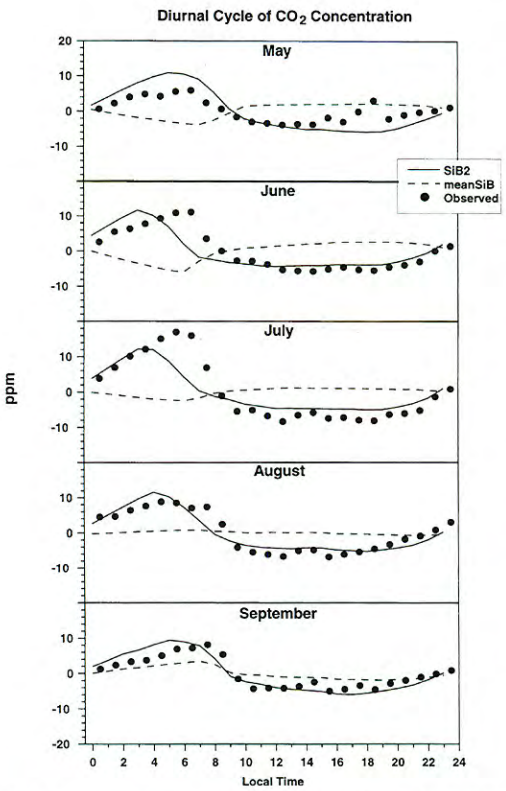


*Fig. 6.* Comparison of simulated and observed monthly composite diurnal cycles of $CO_2$ concentration in the PBL at the site of the BOREAS field experiment for five months. The solid curves show the conentrations simulated using SiB2, and the dashed curves show the concentrations simulated in the meanSiB experiment.

during daylight but soil respiration continues through the night as well. The atmospheric transport of the trace gases has strong diurnal components as well (Fig. 7). Surface heating by the sun drives PBL growth by turbulent entrainment during daylight hours, and cumulus convection (at least over land) shows a strong daytime maximum in most regions. Because photosynthetic drawdown of $CO_2$ is positively correlated with active PBL turbulence, it acts on a deeper layer of air than nighttime respiratory fluxes. Furthermore, the $CO_2$-depleted air in the daytime PBL is much more likely to be carried aloft by cumulus convection than is the $CO_2$-enriched air at night. This pattern is more realistic than in the meanSiB run, which includes depletion of $CO_2$ in the nocturnal PBL, as if the sun were shining 24 hours a day during the growing season. Similarly, in the fall when daily soil respiration exceeds daily NPP, the meanSiB fluxes behave as if photosynthesis is completely absent whereas SiB2 continues to deplete $CO_2$ from the deep PBL in the daytime and enrich the more stable autumn PBL at night. We turn now to an analysis of the simulated seasonal cycle of atmospheric $CO_2$.

## 4. Seasonal cycle

The seasonal cycle of atmospheric $CO_2$ over much of the world is largely driven by the seasonal fluxes at the land surface. The seasonal amplitude at the Earth's surface as simulated by SiB2 is

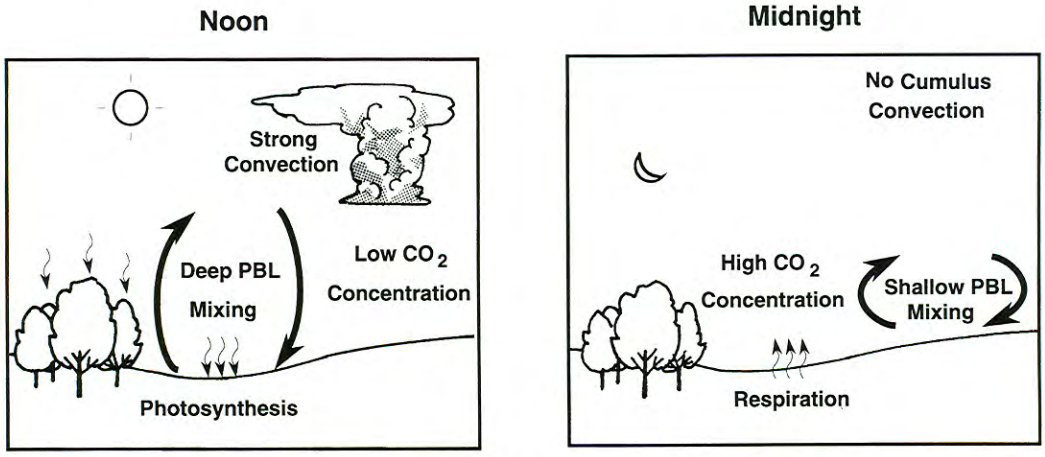


*Fig. 7.* Schematic depiction of diurnal correlations betwee the terrestrial surface fluxes and vertical transport of $CO_2$.

somewhat higher over the continental interiors than as simulated in previous studies (Fung et al., 1987; Heimann et al., 1989), but shows the same general distribution and meridional gradient (Fig. 8a). The difference between the SiB2 and meanSiB experiments (Fig. 8b) reflects the influence of the coupled diurnal cycles of carbon fluxes and atmospheric transport, with the SiB2 results showing a weaker seasonal cycle over most of the temperate land areas.

Because carbon fluxes due to both photosynthesis and respiration are maximum during the temperate growing season, high $CO_2$ concentrations in the nocturnal PBL partly offset the growing season drawdown of $CO_2$ in the SiB2 experiment, but this effect is absent in the meanSiB run. The tendency of a strong diurnal cycle in concentration near the ground to offset he seasonal cycle over land has been noted by Bakwin et al. (1995) in measurements performed on a television tower in North Carolina. They found that there was very little seasonal cycle at 51 m above the ground, but at 496 m the seasonal amplitude was about 15 ppm. The SiB result is more realistic than the meanSiB result in this sense.

The effect of the diurnal cycle is locally very strong, but at distances of more than a few hundred km from local forcing, the amplitude simulated in the meanSiB experiment is nearly indistinguishable from that simulated by SiB2. At the locations of most of the NOAA flask stations, the amplitude of the simulated seasonal cycle agrees well with that derived from the flask data (Fig. 9). At the 4 northernmost stations (ALT, BRW, MBC, and STM), the GCM tends to overestimate the amplitude by about 20%, and at CBA (on the Alaska Peninsula), the model underestimates the observed amplitude by about 30%. In the northern tropics, the model systematically underestimates the observed amplitude by about a third.

The degree to which the model captures the seasonal cycle at many of the flask stations is surprising given that only terrestrial ecosystem fluxes are represented and the stations are chosen to minimize the effects of these fluxes. Some of the discrepancies between the simulated and observed seasonal amplitude are certainly due to the lack of other forcing in the model. In the tropics, for example, seasonal changes in meridional flow associated with the movement of the ITCZ impose a seasonal cycle on atmospheric $CO_2$ because of the strong meridional gradient due to fossil fuel emissions in the northern hemisphere. This effect is apparent in the seasonal time series for several specific stations (Fig. 10). The simulated concentrations are too high from July through November at KUM, RPB, and CHR, when incursions of low-$CO_2$ air from the southern hemisphere are brought northward in the lower branch of the Hadley Cell. The same mechanism may explain the lower-than-observed concentrations simulated at ASC and SMO earlier in the year.

Because vegetation covers so little land area in the southern hemisphere, the weak seasonal cycle at high southern latitudes is probably influenced by other factors such as transport of fossil fuel $CO_2$ and air-sea exchange. Convesely, the seasonal cycle is expected to be dominated by the seasonal terrestrial fluxes at high northern latitudes, so the degree of agreement between the model and the flask data at ALT and BRW (Fig. 10) is encouraging. The simulated concentrations are higher than observed in early spring, when respiration from soils releases $CO_2$ before the growing season really gets started. This "blip" explains the systematic overestimation of seasonal amplitude at the highest latitudes (Fig. 9), but is smaller than has been previously simulated by models forced with seasonal carbon fluxes estimated from satellite imagery and climate data (Fung et al., 1987; Heimann et al., 1989; Tans et al., 1990; Denning, 1994).

The amplitude of the seasonal cycle is observed to decrease with height (Bolin and Bischof, 1970; Pearman and Beardsmore, 1984), and it is clear that the seasonal amplitude has significant spatial structure in the upper troposphere (Tanaka et al., 1987; Nakazawa et al., 1991, 1992). Aircraft observations of seasonal $CO_2$ variations in the upper troposphere may provide an additional constraint on model calculations, but at present such data are available for only a handful of locations. The seasonal amplitude of $CO_2$ simulated using the CSU GCM is considerably weaker in the upper troposphere than at the surface (Fig. 11). The seasonal cycle at 200 mb is modulated by a combination of carbon metabolism and deep cumulus convection, and so is strongest over regions where both biological activity and convec-

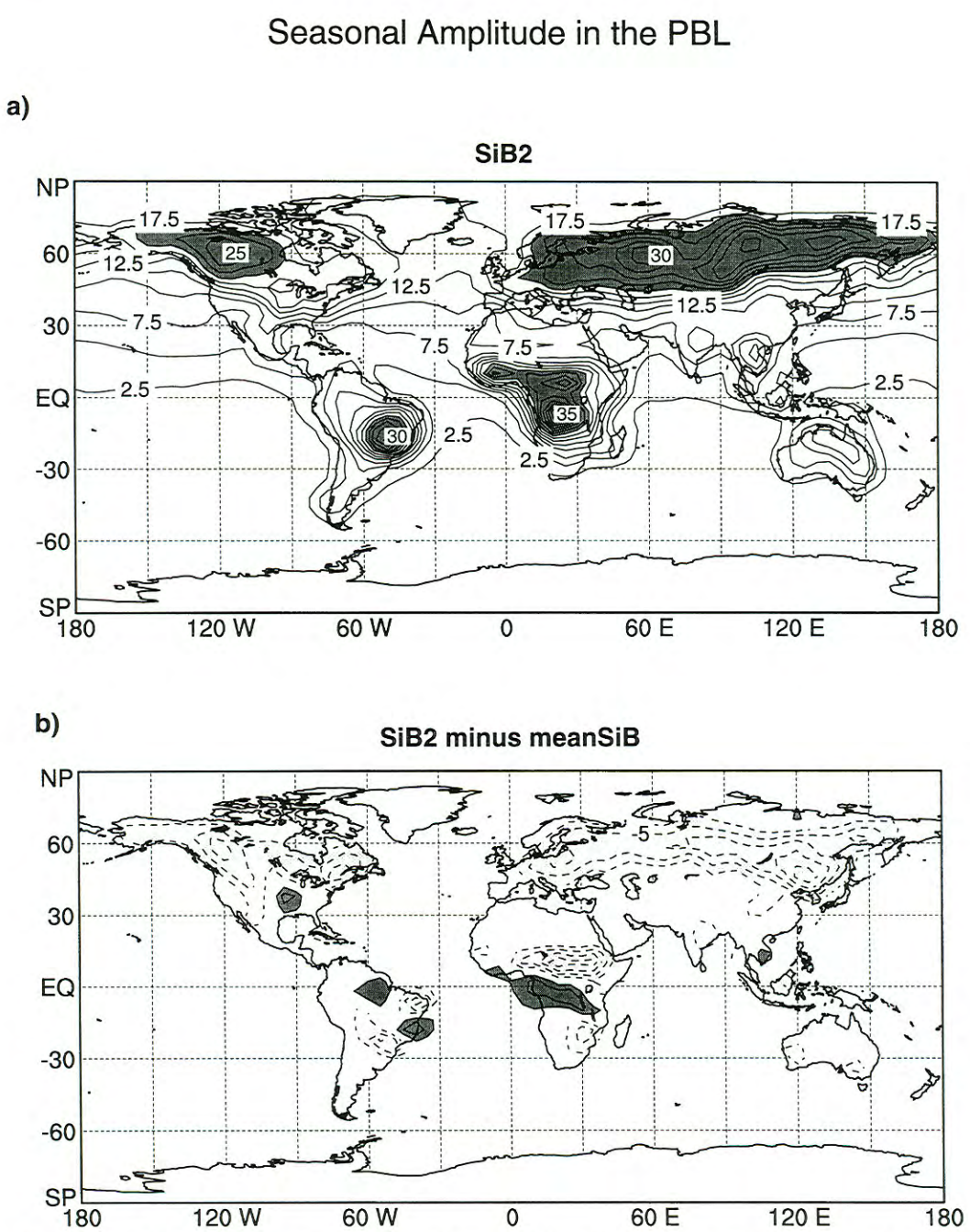


*Fig. 8.* Maps of the amplitude (ppm) of the seasonal cycle of $CO_2$ in the PBL. (a) Simulation using SiB2. Contour interval is 2.5 ppm. Shading indicates values greater than 20 ppm. (b) Difference (SiB2 minus meanSiB). Contour interval is 2.5 ppm, with dark shading for values greater than 2.5 ppm and light shading for values less than −2.5 ppm. The zero contour has been omitted for clarity.

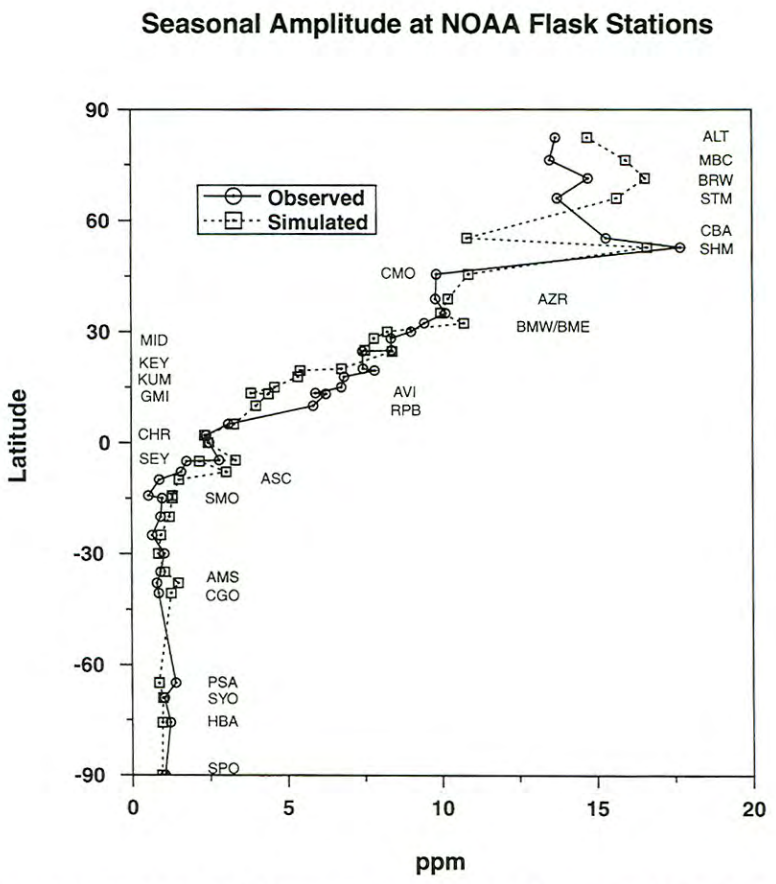


*Fig. 9.* Amplitude of the simulated and observed seasonal cycle of $CO_2$ concentration at 40 stations in the NOAA/CMDL flask sampling network. The flask data were fitted with a linear trend and four seasonal harmoncis, and the fitted function was evaluated for 1990.

tion are strongly seasonal due to the Asian Monsoon.

Unlike the seasonal cycle at the surface, the amplitude of the seasonal cycle aloft is greater in the SiB2 run in which carbon metabolism is diurnal than in the meanSiB experiment with purely seasonal forcing. This reflects the tendency for afternoon maxima in convective activity over land, which preferentially transports $CO_2$-depleted air into the upper troposphere. Neither experiment, however, produces as great a seasonal amplitude ove the western Pacific as reported by Nakazawa et al. (1991) for data collected on commercial airliners between Japan and Australia (Fig. 12). The GCM successfully reproduces the weak amplitude in the southern tropics and the sign of the gradient in the northern hemisphere, but the simulated amplitude near Japan is too small by about a factor of two.

Seasonal changes in vertical and meridional structure of $CO_2$ concentration and atmospheric transport are presented in Fig. 13 and Fig. 14. In January, the $CO_2$ concentration decreases rapidly with height in northern hemisphere (Fig. 13a), due to respiration efflux enriching the lower troposphere. In the southern tropics, a distinct concentration minimum is present in the upper troposphere and lower stratosphere. The simulated mean meridional circulation of the atmosphere is represented in terms of the stream-

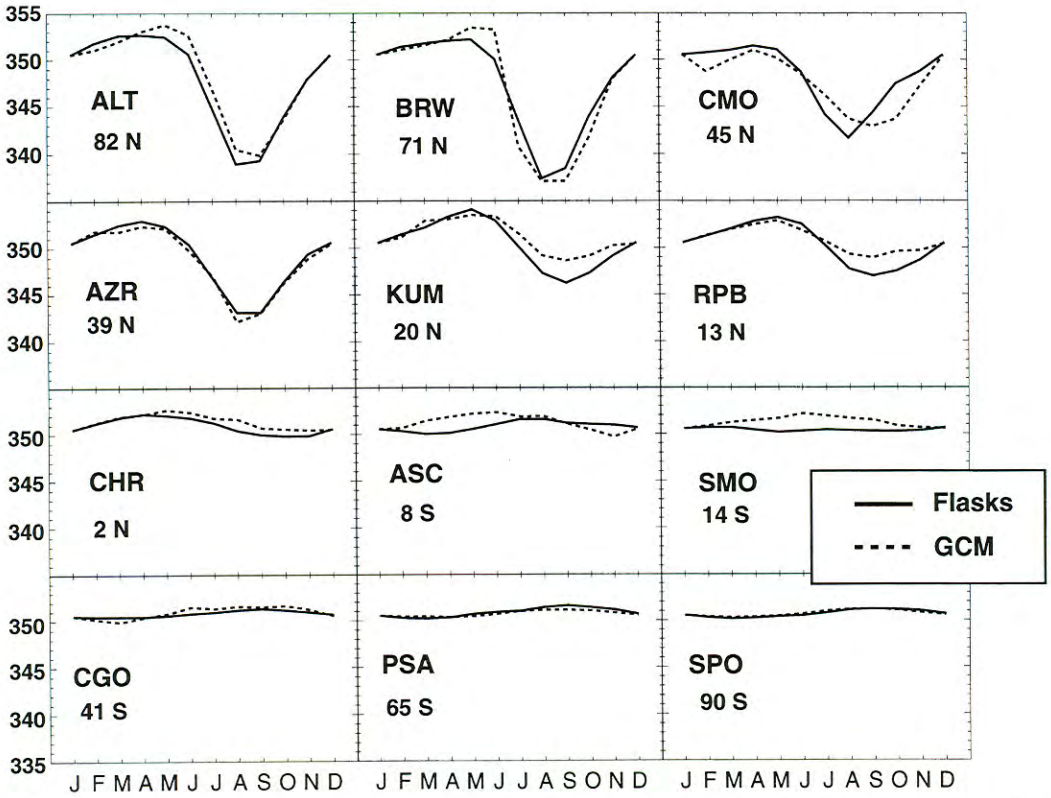


*Fig. 10.* Seasonal time series of simulated (dashed lines) and observed $CO_2$ concentration (solid lines) at 12 stations in the NOAA/CMDL flask network. The flask data were fitted with a linear trend and four seasonal harmonics. Only the seasonal harmonics are represented here. The simulated and observed concentrations are set equal in January, and monthly means are plotted for each month.

function (Fig. 13b), with mass transport by the mean flow following contour lines, and velocities proportional to the gradient. Low-level mass convergence in the southern tropics is predominantly coupled to poleward return flow in the upper troposphere of the northern hemisphere associated with the Hadley cell, with weaker Ferrel circulations present in the middle latitudes of both hemispheres. The product of the mass flux in Fig. 13b and the concentration field in Fig. 13a gives the zonal mean meridional and vertical transport of $CO_2$ by the resolved flow (Fig. 13c). Unlike the case for the overall mass streamfunction, contours intersect the lower boundary of the model, with carbon flowing upward into the atmosphere in regions where respiration dominates, into the ground where photosynthesis dominates, and atmospheric transport from source to sink regions. In January, most of the transport by the mean flow is accomplished in the lower troposphere.

Subgrid-scale vertical transport of $CO_2$ by cumulus convection is mostly confined to the tropics and southern hemisphere in the southern summer (Fig. 13d), adding $CO_2$ to the upper troposphere in the deep tropics and depleting it further south. The tropical pattern of net $CO_2$ transport from the PBL to the upper troposphere reflects the lack of strong seasonality of the surface fluxes there (see Fig. 6 of Part 1), and the accumulation of $CO_2$ at low levels due to the interaction between strong respiration fluxes and the diurnal cycle of PBL turbulence (cf. Fig. 17a). In the deep tropics, the effects of the PBL depth and cumulus convection are at cross purposes, with cumulus convection acting to *reduce* the very strong vertical gradient

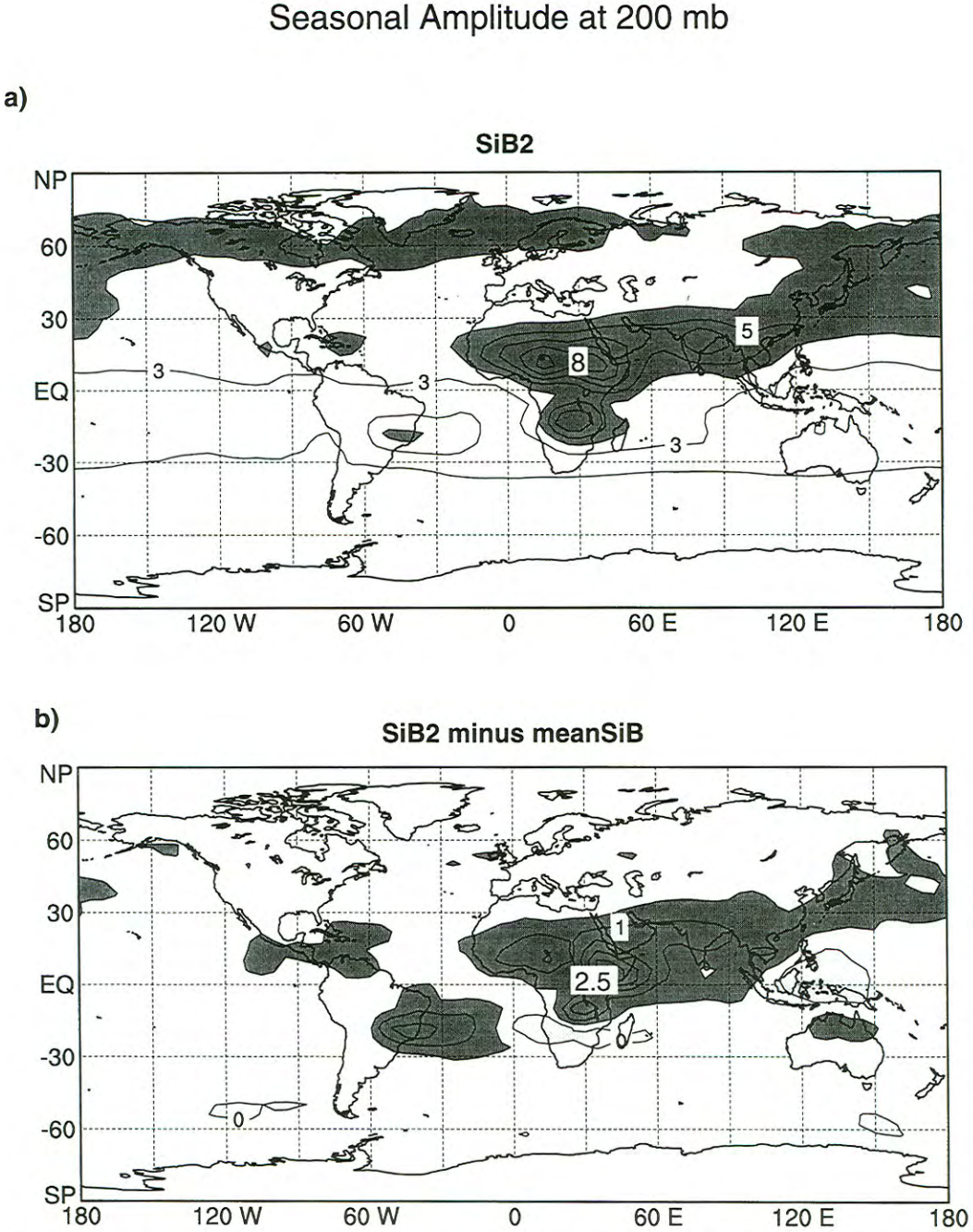


*Fig. 11.* Map of the amplitude (ppm) of the seasonal cycle of $CO_2$ at 200 mb. (a) Simulation using SiB2. Contour interval is 1.0 ppm. Shading indicates values greaer than 4.0 ppm. (b) Effect of the diurnal cycle (difference between SiB2 and meanSiB simulations). Contour interval is 0.5 ppm. Dark shading indicates values greater than 0.5 ppm, and light shading indicates values less than 0.0 ppm.

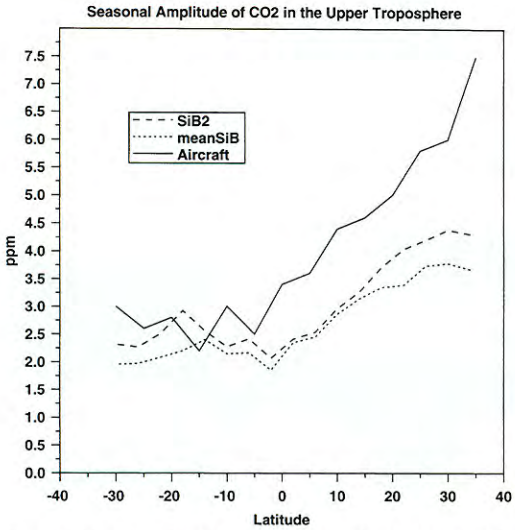


*Fig. 12.* Amplitude of the seasonal cycle of $CO_2$ in the upper troposphere over the western Pacific. The solid line shows the data of Nakazawa et al. (1991). The dashed lines represent the SiB2 and meanSiB simulations at 200 mb and 150° E longitude.

established by the covarying diurnal cycles of PBL depth and ecosystem carbon flux. At 30° S, where seasonal uptake is strong in January, $CO_2$-depleted air is removed from the PBL by cumulus convection and detrained in the upper troposphere. The interaction of cumulus detrainment and meridional transport in the upper troposphere produces the concentration minimum in Fig. 13a. The effect of the diurnal cycle on the global scale transport is to increase the meridional transport by the resolved flow (Fig. 13e) by enhancing the vertical gradient through increased vertical transport of $CO_2$-depleted air by cumulus convection (Fig. 13f). Even in the deep tropics, where the overall influence of cumulus convection is to reduce the vertical gradient, the diurnal covariance of PBL concentrations and cumulus mass flux tends to reduce the $CO_2$ concentration aloft.

In July, $CO_2$ depletion by photosynthesis in the northern hemisphere penetrates much deeper than the enhanced $CO_2$ due to respiration in January (Fig. 14a). Consequently, the resolved transport by the July circulation (Fig. 14b) is also much deeper than was the case in January (Fig. 14c). Note that the simulated mass circulation in the deep southern hemisphere is thermally direct, whereas the real atmosphere is characterized by a thermally indirect Ferrel cell in the austral winter. Subgrid-scale transport by cumulus convection over the northern temperate zone (Fig. 14d) is much more intense in July, tending to reduce the zonal mean $CO_2$ concentration at 50° N and 9 km by more than 34 ppm $yr^{-1}$. As in January, the diurnal coupling between biological activity and transport represented in the GCM acts to enhance the meridional transport by the mean flow (Fig. 14e) by strengthening the subgrid-scale vertical transport and therefore the vertical concentration gradient.

Ecosystem carbon metabolism is most strongly seasonal over the northern temperate and boreal zones (see Part 1), producing the strongest seasonal amplitude in PBL $CO_2$ concentrations. The region is also characterized by very strong seasonality in the activity of moist convection and the depth of PBL turbulence (Fig. 15). Just as the diurnal cycles of photosynthesis and vertical transport in the atmosphere are driven by diurnally varying insolation, the covariance among these variables on the seasonal time scale is driven by common physical forcing (Fig. 16). Deep PBL mixing over terrestrial ecosystems tend to dilute the growing season depletion of $CO_2$ near the surface and strong cumulus convection transports $CO_2$-depleted air to the upper troposphere. Conversely, respiration efflux from the soils is greater than photosynthetic uptake in fall and spring when cold, stable conditions tend to amplify the effect of these fluxes. Cumulus convection is much weaker during those seasons so the $CO_2$-enriched air tends not to be transported to the upper troposphere. This effect was documented by Heimann et al. (1989), who showed that it resulted in an annual mean gradient of several tenths of a ppm in zonal mean $CO_2$ at the surface in the annual mean. Denning et al. (1995) showed that the effect was much stronger in the CSU GCM. In the next section we analyze the impact

*Fig. 13.* Vertical and meridional structure of simulated $CO_2$ and transport for January. Plots are cross sectons of zonal mean values, with latitude on the abscissa (North Pole to the left), and height in km on the ordinate. For clarity, the zero contour has been omitted in all panels except for (a). (a) $CO_2$ concentration (ppm)simulated using SiB2. The three-dimensional, mass-weighted mean concentration has been subtracted. Contour interal is 0.25 ppm for absolute values less than 2 ppm, and 1.0 ppm for absolute values greater than 2 ppm. Dark shading indicates

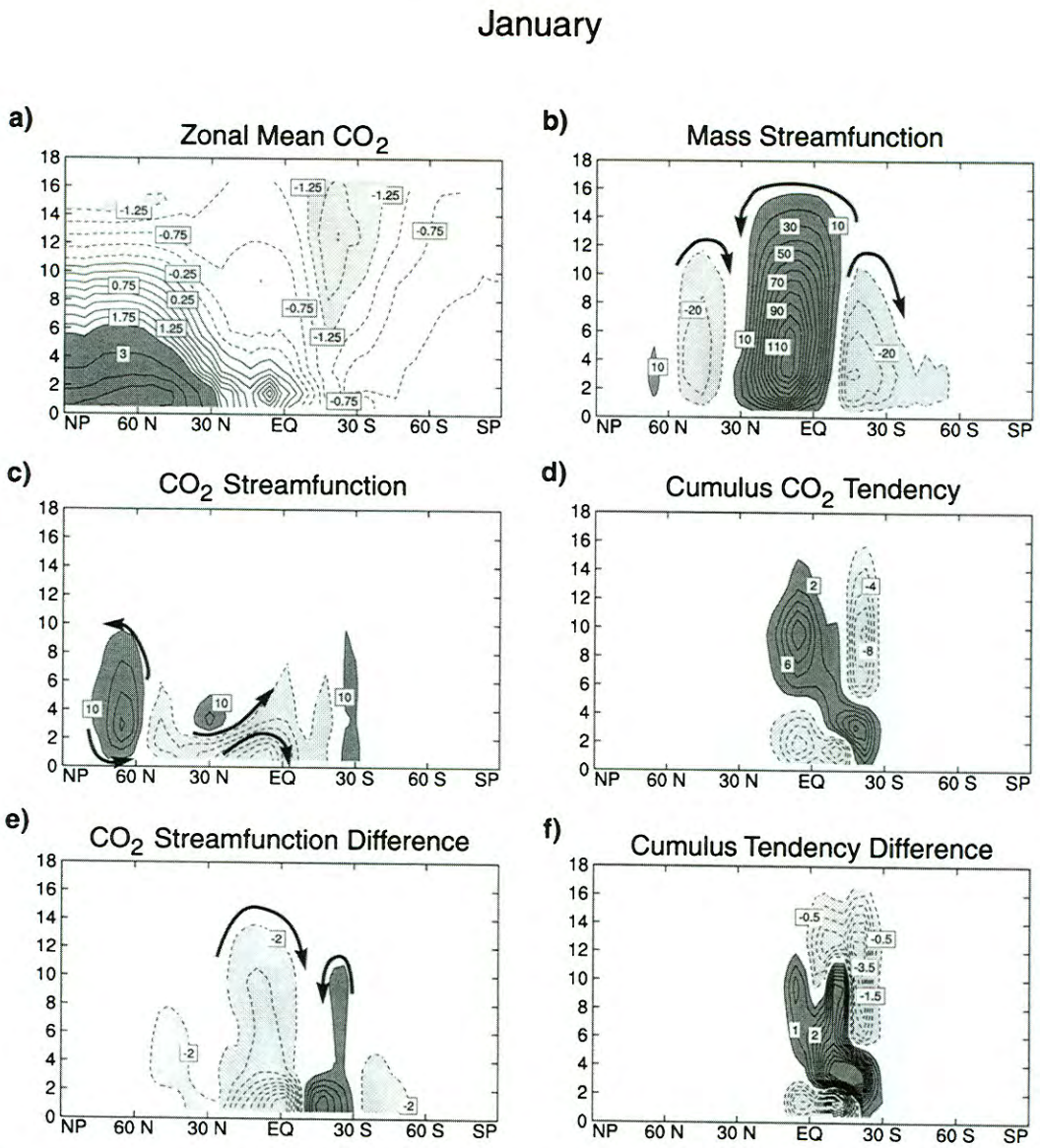


values greater than 2 ppm, and light shading indicates values less than $-1.25$ ppm. (b) Streamfunction of the mean meridional circulation of mass ($10^9$ kg s$^{-1}$). The contour interval is $10 \times 10^9$ kg s$^{-1}$. Dark shading indicates values greater than $10 \times 10^9$ kg s$^{-1}$. Light shading indicates values less than $-10 \times 10^9$ kg s$^{-1}$. (c) Streamfunction of the mean meridional circulation of anomalous $CO_2$ ($10^3$ kg s$^{-1}$). The contour interval is $10 \times 10^3$ kg s$^{-1}$. Dark shading indicates values greater than $10 \times 10^3$ kg s$^{-1}$. Light shading indicates values less than $-10 \times 10^3$ kg s$^{-1}$. (d) Tendency of $CO_2$ concentration (ppm yr$^{-1}$) due to transport by cumulus convection. The contour interval is 2 ppm yr$^{-1}$. Dark shading indicates values greater than 2 ppm yr$^{-1}$. Light shading indicates values less than $-2$ ppm yr$^{-1}$. (e) Effect of the diurnal cycle on the streamfunction of the mean meridional circulation of anomalous $CO_2$ (SiB2 minus meanSiB result, $10^3$ kg s$^{-1}$). Contour interval is $2 \times 10^3$ kg s$^{-1}$. Dark shading indicates values greater than $2 \times 10^3$ kg s$^{-1}$. Light shading indicates values less than $-2 \times 10^3$ kg s$^{-1}$. (f) Effect of the diurnal cycle on the tendency of $CO_2$ due to transport by cumulus convection (SiB2 minus meanSiB result, ppm yr$^{-1}$). Contour interval is 0.5 ppm yr$^{-1}$. Dark shading indicates values greater than 0.5 ppm yr$^{-1}$. Light shading indicates values less than $-0.5$ ppm yr$^{-1}$.

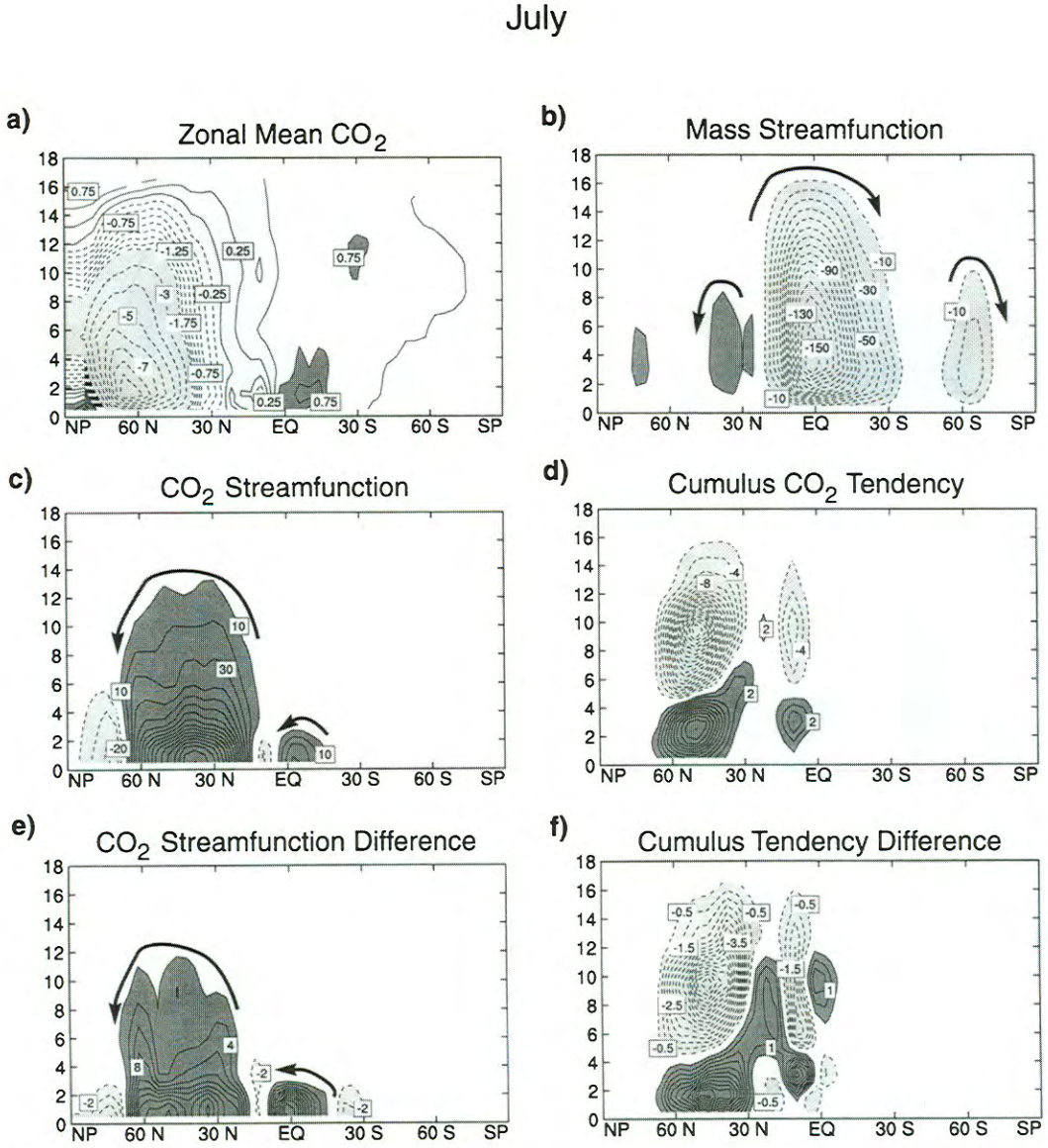


*Fig. 14.* As in Fig. 13, but for July. All contouring and shading is identical to Fig. 13 except in panel (a), where the dark shading indicates values greater than 0.75 ppm, and light shading indicates values less than −2 ppm.

of both the seasonal and diurnal covariance on the annual mean spatial structure and transport of $CO_2$ in the atmosphere.

## 5. Annual mean $CO_2$ distribution

The simulated net exchange of $CO_2$ between the land surface and atmosphere is forced to be nearly in balance (see Subsection 2.2), so spatial gradients in simulated $CO_2$ concentration in the annual mean are entirely due to covariance between carbon fluxes and atmospheric transport (Fung et al., 1983, 1987; Keeling et al., 1989; Denning et al., 1995). Denning et al. (1995) showed that when driven by the purely seasonal surface fluxes of Fung et al. (1987), the CSU GCM

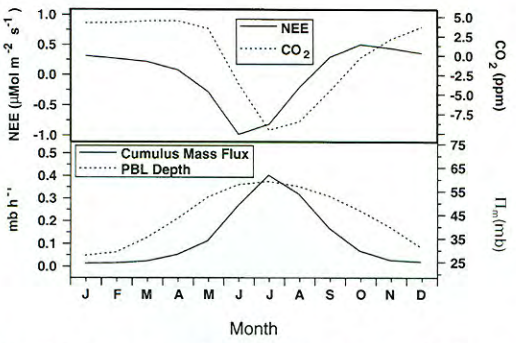


*Fig. 15.* Time series of monthly mean values of selected variables, defining the seasonal cycle over land in the northern temperate and boreal regions. Values are area-weighted means over all land grid points north of 28 N.

produced a much stronger meridional gradient in simulated atmospheric $CO_2$ concentraions than previously simulated using the chemical tracer model (CTM) developed at the Goddard Institute for Space Studies (GISS, Fung et al., 1983, 1987; Tans et al., 1990). The depth of vertical mixing of surface signals in the GISS model varies only in discrete steps, and has a minimum value of 50 mb, which is deeper than observed under stable conditions (Stull, 1988). By contrast, the CSU GCM represents the depth of PBL mixing in a continuous manner, with a minimum value of 10 mb. This allows respiration in stable air to cause much higher concentrations than seen in the GISS model, and leads to higher simulated surface concentrations in the annual mean.

The on-line fluxes calculated using SiB2 produce very strong concentration maxima over the tropical continents (Fig. 17a), with weaker maxima over the temperate and boreal land masses. The maximum values occur in tropical Africa, where annual mean $CO_2$ is as much as 31 ppm greater than at the South Pole. By contrast, the annual mean concentration of $CO_2$ in the PBL simulated in the meanSiB experiment (Fig. 17b) is much lower over the tropics, with a spatial distribution that is remarkably similar to that obtained using previous estimates of monthly carbon fluxes (Fung et al., 1987; Keeling et al., 1989); Denning et al., 1995). Maximum concentrations in the meanSiB experiment occur over the boreal forest, but the meanSiB values are more than twice as high as those obtained using the GISS CTM. The difference between the SiB2 and meanSiB experiments is largest over the tropics, but the annual mean concentrations are enhanced over much of the land surface of the world when the carbon fluxes are calculated on-line relative to those obtained using monthly mean forcing.

The effect of covariance between ecosystem metabolism and atmospheric transport is to partition $CO_2$ in the vertical, with the PBL systematically reflecting the effects of respiration rather than photosynthesis. Over the land area of the world, the simulated annual mean concentration in the

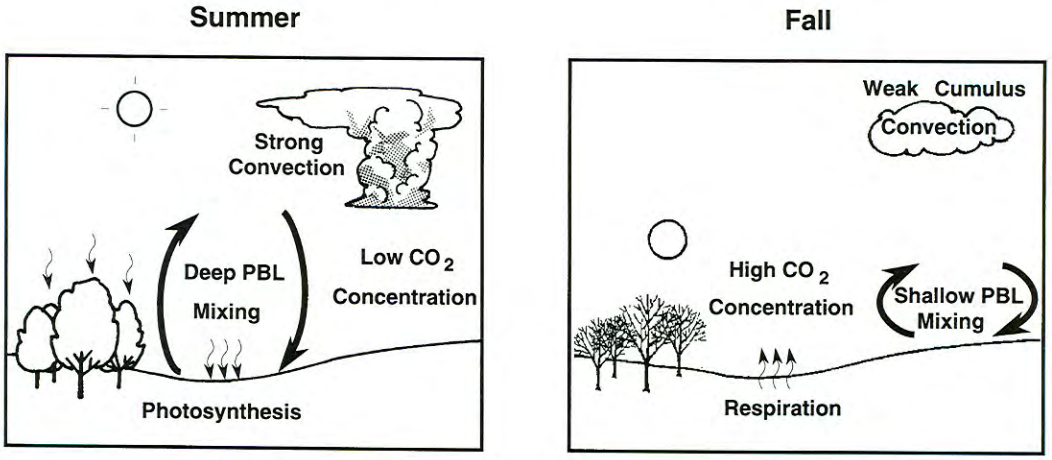


*Fig. 16.* Schematic depiction of seasonal correltions between the terrestrial surface fluxes and vertical transport of $CO_2$.

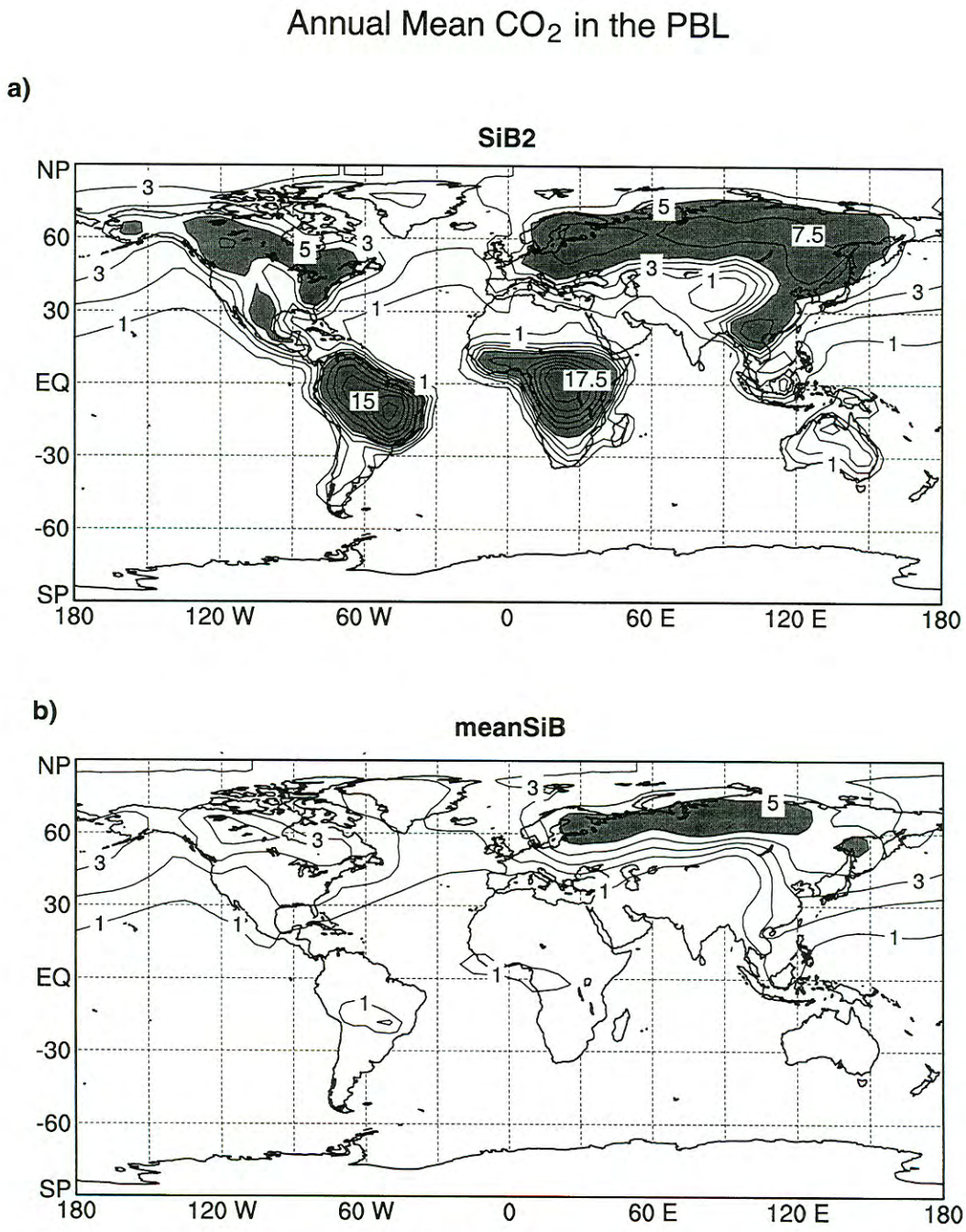


*Fig. 17.* Maps of annual mean $CO_2$ concentration (ppm minus South Pole) in the PBL. In both panels, the contour interval is 1 ppm, for values less than 5 ppm, and 2.5 ppm for values greater than 5 ppm. Shading indicates values greater than 5 ppm. (a) Simulation using SiB2. (b) Simulated using meanSiB.

PBL is correlated with simulated annual NPP ($r=0.82$) (see Part 1). This is due to the fact that respiration is strongest where NPP is greatest. In addition, the diurnal cycle of photosynthesis and respiration in a variable-depth turbulent PBL is active throughout most of the year in the tropics, where seasonality in rainfall rather than temperature determines the "growing season." By contrast the winter months in the boreal forest exhibit almost no net flux.

Unfortunately, very few observational data on $CO_2$ concentrations are available with which to compare the simulated tracer distributions presented in Fig. 17. The annual means presented here represent measurements taken at each grid point once per hour, 24 h a day, 365 days a year. The NOAA flask stations sample only the remote marine PBL, and care is taken to avoid significant local sources. The diurnal cycle has been well documented by intensive field sampling campaigns, but never over very large spatial scales or throughout the year, so the realism of the annual mean fields in Fig. 17 is unknown.

At the locations of the NOAA flask stations, the striking diurnal effects that are evident in Fig. 17 are nearly insignificant. The simulated difference in annual mean $CO_2$ concentration between Alert (82° N) and the South Pole is 3.0 ppm as simulated by SiB2, and 2.7 ppm in the meanSiB experiment. When the CSU GCM was used to transport the fluxes of Fung et al. (1987), the annual mean concentration at Alert was 1.9 ppm greater than at the South Pole (Denning et al., 1995). All of these values are much greater than the Arctic-to-Antarctic gradient of about 0.5 ppm simulated using off-line tracer models (Fung et al., 1983, 1987; Keeling et al., 1989; Tans et al., 1990), and account for a significant fraction of the observed gradient of about 4 ppm in the NOAA record (Conway et al. 1994).

The simulated annual mean vertical distribution of zonal mean $CO_2$ concentration (Fig. 18a) reflects the covariance of vertical transport and surface fluxes. Both the SiB2 and meanSiB results show a strong vertical partitioning of $CO_2$, with enhanced concentrations in the lower troposphere in the northern hemisphere and depleted concentrations aloft. The vertical gradient is about 3 ppm through the depth of the model atmosphere at 60° N. In the annual mean, transport by cumulus convection tends to reduce the concentration of $CO_2$ in the upper troposphere by more than 3 ppm $yr^{-1}$ over the northern temperate and boreal zones (Fig. 18b). Shallow nocturnal and cold-season PBL turbulence concentrates air affected by respiration near the ground, and cumulus convection injects $CO_2$-depleted air affected by photosynthesis into the upper troposphere.

The annual mean vertical gradient of $CO_2$ concentration is only slightly stronger as simulated by SiB2 than in the meanSiB experiment (Fig. 18c). Evidently it is seasonal covariance between surface carbon metabolism and vertical transport that accounts for most of the difference in the vertical structure, with the diurnal effect serving to enhance the effect. This result is also consistent with the weak influence of the diurnal correlations on the annual mean concentrations at the marine flask stations (Fig. 17). Because nocturnal trapping of air affected by respiration is of short duration and confined to only half of a latitude circle at a time, mixing of daytime and nighttime parcels during transport is able to remove most of the signal before continental air reaches the locations of the flask stations. By contrast, the enhancement of $CO_2$ by respiration during the boreal fall and spring is coherent around a latitude circle and persists for weeks, allowing the lower troposphere to become progressively more conentrated in $CO_2$. Similarly, the $CO_2$ concentration in the upper troposphere progressively declines during the boreal growing season as cumulus convection repeatedly deposits $CO_2$-depleted air there. The coupled diurnal cycles of convection and carbon metabolism enhance the seasonal effect by about 20% over the northern middle latitudes.

In Fig. 19, we have added the simulated gradient due to fossil fuel emissions (ALT-SPO = 4.4 ppm (Denning et al., 1995)) to the biogenic gradients simulated in the present study. Also plotted for comparison is the annual mean meridional gradient due to fossil fuels and land vegetation as simulated by Fung et al. (1987) using the GISS tracer model and the observed gradient. Assuming that the model faithfully represents the large-scale meridional transport of trace gases in the atmosphere, the difference between the simulated and observed curves in Fig. 19 represents the influence of all other processes which influence the annual distribution of $CO_2$ at the NOAA flask stations (air-sea exchange and annual net sources and sinks at the land surface). All three simulations with the

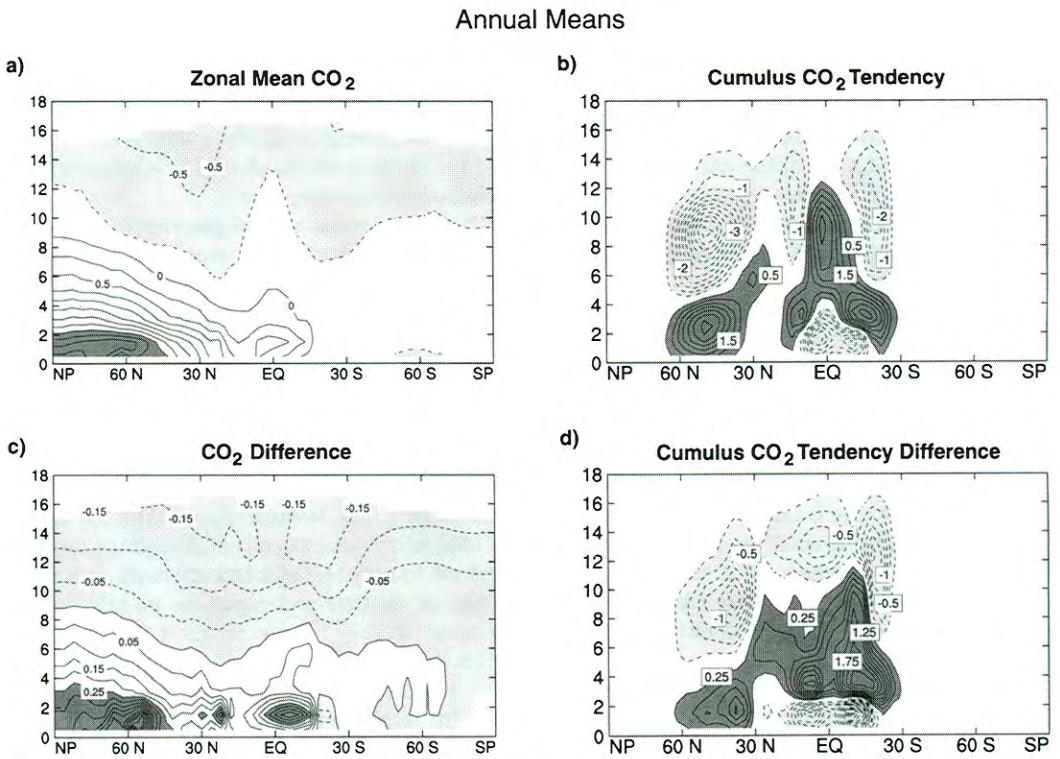


*Fig. 18.* Annual mean vertical and meridional structure in simulated $CO_2$ and $CO_2$ tendency due to transport by cumulus convection. Plots are cross sections of zonal mean values, with latitude on the abscissa (North Pole to the left), and height in km on the ordinate. (a) Simulated $CO_2$ using SiB2. Contour interval is 0.25 ppm. Dark shading indicates values greaer than 2 ppm. Light shading indicates values less than $-0.25$ ppm. (b) Tendency of $CO_2$ concentration (ppm $yr^{-1}$) due to transport by cumulus convection in the SiB2 experiment. The contour interval is 0.5 ppm $yr^{-1}$. Dark shading indicates values greater than 0.5 ppm $yr^{-1}$. Light shading indicates values less than $-0.5$ ppm $yr^{-1}$. The zero contour has been omitted. (c) Effect of the diurnal cycle on the simulated $CO_2$ concentration (difference between SiB2 and meanSiB results, ppm). Contour interval is 0.05 ppm. Dark shading indicates values greater than 0.25 ppm. Light shading indicates values less than 0 ppm. (d) Effect of the diurnal cycle on the tendency of $CO_2$ concentration (ppm $yr^{-1}$) due to transport by cumulus convection (difference between SiB2 and meanSiB results, ppm $yr^{-1}$). The contour interval is 0.25 ppm $yr^{-1}$. Dark shading indicates values greater than 0.25 ppm $yr^{-1}$. Light shading indicates values less than $-0.25$ ppm $yr^{-1}$. The zero contour has been omitted.

CSU GCM (using the SiB2, meanSiB, and the Fung et al., 1987 fluxes) require a much larger net sink in the northern hemisphere than the GISS simulation, and for any given scenario of air-sea exchange in the present study can not be explained by weak meridional transport in the CSU GCM as compared to the GISS tracer model, as there is almost no difference in the simulated spatial structure of fossil fuel $CO_2$ (Denning et al., 1995).

Quantitative estimation of the strength of the sink implied by Fig. 19 is beyond the scope of the present paper. The implied sink varies with the strength of the simulated meridional gradient at the NOAA flask stations, and so with the strength of the seasonal and diurnal covariance between ecosystem metabolism and atmospheric transport in the GCM. The GCM tends to underestimate the amplitude of both the seasonal and diurnal cycles of NEE due to a mismatch between the simulated and real world climate (see Part 1). Unless the model significantly overestimates the seasonality of PBL turbulence and/or transport by cumulus convection, it is likely that the meridional gradients shown in Fig. 19 (and therefore the carbon sink estimated from them) are a lower bound rather than an overestimate.

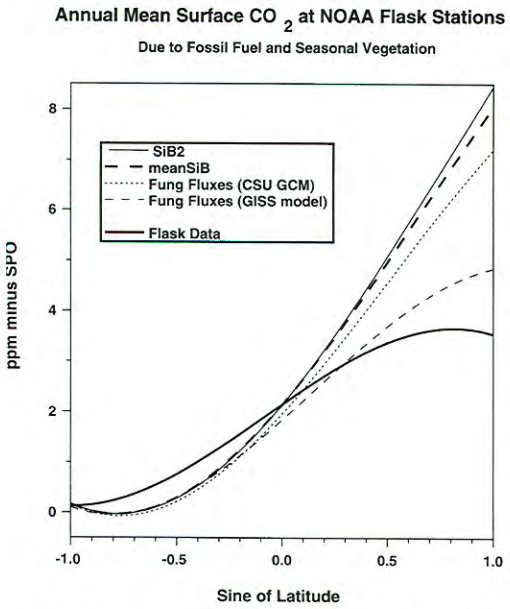


*Fig. 19.* Meridional profiles of annual mean surface $CO_2$ concentration (ppm) at 40 stations in the NOAA/CMDL flask sampling network. All curves are cubic polynomials fitted to the station values. The heavy solid line represents the flask observations, and the four other curves represent different simulations of the meridional gradient arising from fossil fuel emissions (as simulated by Denning et al, 1995) plus seasonal exchange with the terrestrial biosphere. The flask data at each station were fitted with a linear trend and four seasonal harmonics, and the annual mean of each fitted function evaluated for 1990 was used to calculate the heavy solid curve.

## 6. Summary and conclusions

We have successfully simulated many aspects of the temporal and spatial variations of atmospheric $CO_2$ in a coupled model that includes the calculation of both the fluxes and the transport. This is the first such simulation.

The use of a short time step that fully resolves the diurnal cycle of the carbon fluxes as well as important aspects of the atmospheric circulation provides a much higher degree of realism in terms of the validation data considered here than when the model is forced by monthly mean fluxes calculated off-line (even though the means were identical). In particular, the use of diurnally varying turbulent mixing in the PBL with the meanSiB fluxes produces simulated diurnal cycles which are much weaker than and nearly 180° out of phase with both the observations and the SiB2 simulation. This inevitably leads to other discrepancies related to diurnally varying transport in the atmosphere, such as a tendency of cumulus convection to pump $CO_2$-enriched rather than $CO_2$-depleted air into the upper troposphere.

The seasonal cycle simulated by the coupled model is somewhat stronger at many locations than previously simulated, but because regular monitoring of atmospheric $CO_2$ is largely confined to remote marine locations remote from direct seasonal forcing, it is impossible to evaluate the realism of this feature. When the model is forced with the monthly mean carbon fluxes, the seasonal cycle at the surface is even stronger over the continents. Both the SiB2 and meanSiB experiments reproduce the seasonal amplitude at the NOAA flask stations fairly well, although the agreement is marginally better in the SiB2 run. The seasonal amplitude in the upper troposphere is generally stronger in the SiB2 (diurnal) experiment than in the meanSiB run, reflecting the greater vertical transport of air that has been depleted of $CO_2$ by photosynthesis due to the diurnal effects noted above. Neither simulation exhibits as great a seasonal amplitude over the western Pacific as the aircraft observations.

In the annual mean, the effect of covariance between the carbon fluxes and atmospheric transport is to concentrate $CO_2$ near the Earth's surface and to deplete it in the upper troposphere. The near surface horizontal structure is determined mostly by interaction between NEE and PBL turbulence, whereas the spatial structure in the upper troposphere is driven by interactions between NEE, penetrative convection, and the mean flow. Most of this effect (about 80%) is due to seasonal covariance, with the coupled diurnal cycles of metabolism and transport acting to reinforce the spatial structure. The diurnal covariance effect imposes very strong regional maxima in PBL concentration where biological activity is strongest (over the tropical rainforests).

At the remote marine locations of the flask sampling stations, the meridional gradient of annual mean $CO_2$ concentration using the SiB2 fluxes is much stronger than previously simulated, implying a qualitatively different picture of the annual carbon budget of the atmosphere than has been previously believed. Our results suggest that the seasonal "breathing" of the terrestrial bio-

sphere plays an active role in determining the annual mean distribution of $CO_2$.

## Acknowledgments

We thank Peter Bakwin of the NOAA/CMDL Carbon Cycle Group, who provided the concentration data for the North Carolina television tower. Prof. Steven C. Wofsy of Harvard University allowed the use of unpublished data collected at the BOREAS Northern Study Area. The flask station data were provided by Tom Conway and Pieter Tans, through the NOAA/CMDL/CCG archive. We thank Donald Dazlich for technical help with the GCM and Kelley Wittmeyer for computer support. Joseph Berry and Inez Fung contributed their wisdom through many spirited discussions.

This research was funded by a NASA Global Change Fellowship, Grant NGT-30150, and under NASA Contract NAS5-31730. Computing resources were provided by the NASA Center for Computational Sciences.

## REFERENCES

Arakawa, A., and Schubert, W. H. 1974. Interaction of a cumulus cloud ensemble with the large-scale environment, Part 1. *J. Atmos. Sci.* **31**, 674–701.

Arakawa, A. and Lamb, V. R. 1977. Computational design of the basic dynamical processes of the UCLA general circulation model. *Methods in Computational Physics* **17**, 173–265.

Bakwin, P. S., Tans, P. P., Zhao, C., Ussler, W. and Quesnell, E. 1995. Measurements of carbon dioxide on a very tall tower. *Tellus* **37**, 535–549.

Bolin, B. and Bischof, W. 1970. Variations of the carbon dioxide content of the atmosphere in the northern hemisphere. *Tellus* **22**, 431–442.

Conway, T. J., Tans, P. P., Waterman, L. S., Thoning, K., Kitzis, D. R., Masarie, K. A. and Zhang, N. 1994. Evidence for interannual variability of the carbon cycle from the NOAA/CMDL global air sampling network. *J. Geophys. Res.* **99**, 22831–22855.

Denning, A. S. 1994. Investigations of the transport, sources, and sinks of atmospheric $CO_2$ using a general circulation model. *Atmospheric Science Paper* **564**, Colorado State University.

Denning, A. S., Fung, I. Y. and Randall, D. A. 1995. Latitudinal gradient of atmospheric $CO_2$ due to seasonal exchange with land biota. *Nature* **376**: 240–243.

Denning, A. S., Collatz, G. J., Zhang, C., Randall, D. A., Berry, J. A., Sellers, P. J., Colello, G. D. and Dazlich, D. A. Simulations of terrestrial carbon metabolism and atmospheric $CO_2$ in a general circulation model. Part 1: Surface carbon fluxes. *Tellus* **48B**, this issue.

Enting, I. G. and Mansbridge, J. V. 1989. Seasonal sources and sinks of atmospheric $CO_2$. Direct inversion of filtered data. *Tellus* **39B**, 318–325.

Enting, I. G. and Mansbridge, J. V. 1991. Latitutindal distribution of sources and sinks of $CO_2$: Results of an inversion study. *Tellus* **43B**, 156–170.

Enting, I. G., Trudinger, C. M. and Francey, R. J. 1995. A synthesis inversion of the concentration and delta $^{13}C$ of atmospheric $CO_2$. *Tellus* **47B**, 35–52.

Fan, S.-M., Wofsy, S. C., Bakwin, P. S., Jacob, D. J. and Fitzjarrald, D. R. 1990. Atmosphere-biosphere exchange of $CO_2$ and $O_3$ in the central Amazon forest. *J. Geophys. Res.* **95**, 16851–16864.

Fowler, L. A. and Randall, D. A. 1996. Liquid and ice cloud microphysics in the CSU General Circulation Model. Part II: Impact on cloudiness, the Earth's radiation budget, and the general circulation of the atmosphere. *J. Clim.* **9**, 530–560.

Fung, I., Prentice, K., Matthews, E., Lerner, J. and Russell, G. 1983. Three-dimensional tracer model study of atmospheric $CO_2$: Response to seasonal exchanges with the terrestrial biosphere. *J Geophys. Res.* **88**, 1281–1294.

Fung, I. Y., Tucker, C. J. and Prentice, K. C. 1987. Application of very high resolution radiometer vegetation index to study atmosphere-biosphere exchange of $CO_2$. *J. Geophys. Res.* **92**, 2999–3015.

Heimann, M. and Keeling, C. D. 1989. A three-dimensional model of atmospheric $CO_2$ transport based on observed winds (2). Model description and simulated tracer experiments. In: D. H. Peterson (ed.): Aspects of climate variability in the Pacific and Western Americas. *Geophysical Monograph* **55**. American Geophysical Union, Washington, DC, 237–275.

Heimann, M., Keeling, C. D. and Tucker, C. J. 1989. A three-dimensional model of atmospheric $CO_2$ transport based on observed winds (3). Seasonal cycle and synoptic time scale variations. In: Aspects of climate variability in the Pacific and Western Americas. *Geophysical Monograph* **55** (ed. D. H. Peterson). American Geophysical Union, Washington, DC., 277–303.

Keeling, C. D., Piper, S. C. and Heimann, M. 1989. A three-dimensional model of atmospheric $CO_2$ transport based on observed winds (4). Mean annual gradients and interannual variations. In: Aspects of climate variability in the Pacific and Western Americas. *Geophysical Monograph* **55** (ed. D. H. Peterson). American Geophysical Union, Washington, DC., 305–363.

Lord, S. J., Chao, W. C. and Arakawa, A. 1982. Interaction of a cumulus cloud ensemble with the large-scale environment. Part IV. The discrete model. *J. Atmos. Sci.* **39**, 104–113.

Manabe, S., Smagorinsky, J. and Strickler, R. 1965. Simulated climatology of a general circulation model with a hydrologic cycle. *Mon. Wea. Rev.* **93**, 769–798.

Nakazawa, T., Miyashita, K., Aoki, S. and Tanaka, M. 1991. Temporal and spatial variations of upper tropospheric and lower stratospheric carbon dioxide. *Tellus* **39B**, 106–117.

Nakazawa, T., Murayama, S., Miyashita, K., Aoki, S. and Tanaka, M. 1992. Longitudinally different variations of lower tropospheric carbon dioxide concentrations over the North Pacific Ocean. *Tellus* **44B**, 161–172.

Pearman, G. I. and Hyson, P. 1980. Activities of the global biosphere as relflected in atmospheric $CO_2$ records. *J. Geophys. Res.* **85**, 4468–4474.

Pearman, G. I., Hyson, P. and Fraser, P. J. 1983. The global distribution of atmospheric carbon dioxide (1). Aspects of observations and modeling. *J. Geophys. Res.* **88**, 3581–3590.

Pearman, G. I. and Beardsmore, D. J. 1984. Atmospheric carbon dioxide measurements in the Australian region: 10 years of aircraft data. *Tellus* **36B**, 1–24.

Pearman, G. I. and Hyson, P. 1986. Global transport and inter-reservoir exchange of carbon dioxide with particular reference to stable isotopic distributions. *J. Atmos. Chem.* **4**, 81–124.

Randall, D. A., Harshvardhan, Dazlich, D. A. and Corsetti, T. G. 1989. Interactions among radiation, convection, and large-scale dynamics in a general circulation model. *J. Atmos. Sci.* **46**, 1943–1870.

Randall, D. A., Harshvardhan and Dazlich, D. A. 1991. Diurnal variability of the hydrologic cycle in a general circulation model. *J. Atmos. Sci.* **48**, 40–62.

Randall, D. A., Shao, Q. and Moeng, C.-H. 1992. A second-order bulk boundary-layer model. *J. Atmos. Sci.* **49**, 1903–1923.

Randall, D. A. and Pan, D.-M. 1993. Implementation of the Arakawa-Schubert parameterization with a prognostic closure. In: *The representation of cumulus convection in numerical models* (eds. K. Emanuel and D. Raymond). American Meterological Society, Boston, 137–144.

Randall, D. A., Sellers, P. J., Berry, J. A., Dazlich, D. A., Zhang, C., Collatz, G. J., Denning, A. S., Los, S. O., Field, C. B., Fung, I., Justice, C. O. and Tucker, C. J. 1996. A revised land-surface parameterization (SiB2) for GCMs. Part 3: The greening of the Colorado State University General Circulation Model. *J. Clim.* **9**, 738–763.

Rood, R. B. 1987. Numerical advection algorithms and their role in atmospheric transport and chemistry models. *Rev. Geophys* **25**, 71–100.

Sellers, P. J., Hall, F. G., Margolis, H., Kelly, B., Baldocchi, D., den Hartog, G., Chilar, J., Ryan, M. G., Goodison, B., Crill, P., Ranson, K. J., Lettenmaier, D. and Wickland, D. 1995. The boreal ecosystem-atmosphere study (BOREAS). An overview and early results from the 1994 year. *Bull. Amer. Meteorol. Soc.* **76**, 1549–1577.

Sellers, P. J., Randall, D. A., Collatz, G. J., Berry, J., Field, C., Dazlich, D. A., Zhang C. and Bounoua, L. 1996. A revised land-surface parameterization (SiB2) for atmospheric GCMs. Part 1. Model formulation. *J. Clim.* **9**, 676–705.

Stephens, G. L., Randall, D. A., Tjemkes, S. J., Wittmeyer, I. M. and Dazlich, D. A. 1993. The Earth's radiation budget in relation to the hydrologic cycle. Part III. Comparison of observations with a GCM. *J. Geophys. Res.* **98**, 4931–4950.

Stull, R. B., 1988. *An introduction to boundary layer meteorology*. Kluwer Academic Publishers, Dordrecht, The Netherlands.

Suarez, M. J., Arakawa, A. and Randall, D. A. 1983. Parameterization of the planetary boundary layer in the UCLA general circulation model: Formulation and results. *Mon Wea. Rev.* **111**, 2224–2243.

Tanaka, M., Nakazawa, T. and Aoki, A. 1987. Time and space variations of tropospheric carbon dioxide over Japan. *Tellus* **39B**, 3–12.

Tans, P. P., Conway, T. J. and Nakazawa, T. 1989. Latitudinal distribution of the sources and sinks of atmospheric carbon dioxide derived from surface observations and an atmospheric transport model. *J. Geophys. Res.* **94**, 5151–5172.

Tans, P. P., Fung, I. Y. and Takahashi, T. 1990. Observational constraints on the global atmospheric $CO_2$ budget. *Science* **247**, 1431–1438.

Wofsy, S. C., Harriss, R. C. and Kaplan, W. A. Carbon dioxide in the atmosphere over the Amazon Basin. *J. Geophys. Res.* **93**, 1377–1387, 1988.